TECHNICAL MEMORANDUMS

NATIONAL ADVISORY COMMITTEE FOR AERONAUTICS

No. 1061

ANALYSIS OF EXPERIMENTAL INVESTIGATIONS OF THE PLANING PROCESS ON THE SURFACE OF WATER

By W. Sottorf

Jahrbuch 1937 der Deutschen Luftfahrtforschung

Washington
March 1944

NATIONAL ADVISORY COMMITTEE FOR AERONAUTICS

TECHNICAL MEMORANDUM NO. 1061

ANALYSIS OF EXPERIMENTAL INVESTIGATIONS OF THE PLANING PROCESS ON THE SURFACE OF WATER*

By W. Sottorf

Pressure distribution and spray measurements were carried out on rectangular flat and V-bottom planing surfaces. Lift, resistance, and center-of-pressure data are analyzed and it is shown how these values may be computed for the pure planing process of a flat or V-bottom surface of arbitrary beam, load and speed, the method being illustrated with the aid of an example.

SUMMARY

Flat and V-bottom longitudinally straight planing surfaces are investigated. For such surfaces the total resistance may, for a given lift, be separated into a normal and frictional component. The analysis of the tests leads to representations of the lift and center-of-pressure position as functions of the aspect ratio of the pressure area with the Froude number, which characterizes the effect of gravity, as parameter. While the frictional resistance coefficient is equal to that given by Prandtl for the turbulent boundary layer with preceding laminar layer. For high Froude numbers, for which the contribution of gravity to the lift is negligibly small, there is shown to be an agreement between the planing surface tests and the lift on flat airfoils on the under side. The deviations from the Wagner theory for short plates at large aspect ratios are considerable though justified by the conditions neglected in the theory.

With the aid of a working chart a number of practical examples are computed that provide the answers to several important questions. For the case of the flat plate the width of the plate, which is always the full width of the planing surface has an effect on the resistance-load ratio in that the latter becomes more favorable with increasing width.

---

*"Analyse experimenteller Untersuchungen über den Gleitvorgang an der Wasseroberfläche." Jahrbuch 1937 der deutschen Luftfahrtforschung, pp. I 320 – I 339.

With regard to the load effect, on account of the impairment in the aspect ratio, there is an impairment in the resistance-load ratio with increasing load.

With regard to the effect of the speed, however, on account of the improvement in the aspect ratio with increasing dynamic pressure above the first resistance maximum, there is an improvement in the resistance-load ratio with increasing speed.

The tests for the scale effect show that there is similarity of the pressure surfaces and pressure distribution and that the effect of the scale is given only by the dependence of the friction coefficient on the Reynolds number. Only for very small dimensions and loads of the planing surfaces does non-similarity occur in the flow conditions because of the effect of surface tension.

The impairment in the resistance-load ratio by the effect of the V bottom is also shown. With regard to the effect of the width it is found for the V bottom that at small load or high dynamic pressure and with the "natural width," which is less than that of the planing surface, an optimum width occurs which is to be determined for each particular case.

INTRODUCTION

When, with the development of aircraft, the investigation and development of seaplane floats were added to the usual problems of the towing tank, there was a lack of theoretical as well as experimental underlying bases for evaluating the test results. A first experiment with a flat planing surface was carried out in 1912 in England at the William Froude Laboratory and a report was presented by Baker and Millar (reference 1), who, however, did not continue any further work of fundamental investigation. In order to create a sufficiently wide basis, tests on planing surfaces have been conducted by the author since 1928 at the Hamburg Ship Construction Experimental Institute. Starting with tests on a flat rectangular planing surface which served for the study of the planing process and its effect on the fluid surface the test program was later extended so that answers

could be furnished to the most important questions arising for the constructor and research engineer: namely, the effect of the beam, loading, speed, and V angle on the resistance and the effect of the scale in applying the model test results to the full-scale design. These questions may be answered from the results of planing surface tests insofar as the pure planing condition is being considered, this condition being characterized in a float by the breaking away of the water at the step and side edges of the portion of the bottom in front of the step and also by the breaking of the water contact at the stern. (See reference 2.) The results were partially published in the following years (reference 3). Meanwhile, since a theoretical treatment of the actual planing process that takes all conditions into account does not appear possible, Wagner (reference 4) concerned himself with the limiting cases of the planing process (high speed planing-neglecting gravity, and infinitely small trim angles) and by the application of the airfoil comparison, presented an approximate experimental method that enabled him to determine the forces and wetted surface of the flat plate with small aspect ratio also for finite trim angles. The comparison of the first test results of the author with the Wagner theory showed that in the range of small aspect ratios rough agreement was obtained while for large aspect ratios the deviation from the theory was considerable. Wagner ascribed this deviation to the effect of gravity. Sambraus (reference 5) carried out supplementary tests at higher speeds at the Prussian Experimental Institute for Ship Constitution in order to test the Wagner theory also with neglect of gravity for higher aspect ratios. From his result Sambraus concluded that the Wagner theory holds true at high planing speeds for all aspect ratios. Shoemaker (reference 6) likewise extended the range of investigation by towing a series of flat and V-bottom planing surfaces in the NACA tank.

In the take-off of a seaplane the low-speed planing stage, during which gravity exerts a considerable effect, is of equal importance with the high-speed planing stage. The analysis, presented in this paper, of all the author's own tests as well as those of Sambraus and Shoemaker, leads to a clear explanation of the effect of gravity and hence to the representations of lift, resistance and center of pressure, and with the aid of this analysis these values may be numerically determined for flat and V-bottom planing surfaces of arbitrary beam and

arbitrary loading and speed for the condition of pure planing.

NOTATION

A	total lift = load (kg)
A_{dyn}	dynamic lift (kg)
A_{stat}	static lift (kg)
G	total weight (kg)
W	resistance (kg)
W_N	normal resistance (kg)
W_R	frictional resistance (kg)
S	propeller thrust (kg)
Z	towing pull (kg)
N	normal forces (kg)
T	tangential force (kg)
V	static displacement (m^3)
E	load reduction (kg)
$M_{h\,st}$	moment about the lateral axis through step (trailing edge for flat surface, after end of keel for V-bottom surface) (mkg)
v	speed (m/s)
v_m	mean velocity of the water along the planing surface (m/s)
v_o	mean vertical velocity of the mass of water displaced (m/s)
$F = v/\sqrt{g\,b}$	Froude number referred to a fixed dimension of the body

$F^* = v/\sqrt{g\,(A/\gamma)^{1/3}}$ Froude number referred to a length corresponding to the load

$R = v\,l/\nu$ Reynolds number

$\epsilon = W/A$ "Planing Number" resistance-load ratio

$c_a' = \frac{A}{\gamma b^3}, \frac{G}{\gamma b^3 St}$ load coefficient

$c_a = \frac{A}{F\,q}$ lift coefficient of the airfoil

$c_a^* = \frac{A}{l\,b\,q}$ lift coefficient of the planing surface

$c_\alpha = \frac{c_a^*}{\alpha}$ derived lift coefficient of the planing surface

$c_B^* = \frac{A}{(A/\gamma)^{2/3}\,q}$ load coefficient

$c_B = \frac{A}{b^2 q}$ load coefficient

$c_f,\ c_f' = \frac{W_R}{F\,q}$ frictional coefficient

$c_{mh} = \frac{M_h\,St}{\gamma\,b^4}$ moment coefficient

$c_{mh}^* = \frac{M_h\,St}{A\,(A/\gamma)^{1/3}}$ moment coefficient

$q = \rho/2\ v^2$ dynamic pressure (kg/m^2)

ρ density ($kg\ s^2/m^4$)

γ specific weight (kg/m^3)

ν kinematic viscosity (m^2/s)

p, p_{dyn}, p_{stat} pressure (kg/m^2)

p_m mean pressure on "pressure area" (kg/m^2)

l mean length of wetted surface (m)

l_m mean length of pressure area for V-bottom planing surface (m)

l_p distance of center of pressure from trailing edge of planing surface (m)

z local elevation (m)

F wetted surface, also pressure area for flat planing surface (m^2)

F_D projection of pressure area for V-bottom planing surface (m^2)

F wing area (m^2)

b beam of planing surface

b_{st} beam of float at step (m)

b_{nat} natural width of pressure area for V-bottom surface (m)

c distance of fountain from trailing edge of planing surface (m)

α trim

λ scale of model

β dead rise angle

ζ V-angle

EXPERIMENTAL PROCEDURE

Measurement of the Forces

Measurements were made on the lift, resistance, and moment about a lateral axis. The three-component measuring gear is schematically shown in figure 1. The resistance tension wire leads forward from the point P_0, through which passes the axis of the model head, to the dynamometer. The resistance measurement is made by means of a recording pen and coarse weight, the spring force being determined from the record of the spring extension, the spring having been previously calibrated. A constant weight serves to maintain the tautness of the tension member. The calibration wire, in addition, takes up by means of a stop the inertia force that is set up on the model on braking the towing carriage. At equal distances from P_0 there are attached the vertical tension wires leading to the moment beam. With the aid of a sliding weight the moment applied to the model and hence the trim angle may be varied. At P_0 there is attached an additional vertical wire that leads to the unloading beam. By varying the size or the position of the sliding weight the load on the model is reduced so that the remaining weight corresponds to the loading desired. One of the reversing wheels is formed as a gear wheel and to this is attached by means of a coupling, a winch by means of which the model at the end of each test run is lifted from the water in order to remove it from the following waves and utilize the time of the return trip of the carriage for quieting the water surface.

At the start of each test run the model is released only when the dynamic lift is sufficient to avoid an undercutting of the leading edge of the planing surface.

The draft and trim of the model were determined from two draft scales attached to the wheels of the moment balance. The setting for a given trim angle is obtained by displacement of the sliding weight of the moment balance and reading of an angle-indicating device. Damping when required is exerted at the dynamometer lever (damping of longitudinal oscillations) and at the slide of the moment balance (damping of vertical oscillations).

The relative air velocity at the location of the model is, on account of the closed carriage and two air scoops, practically equal to zero so that the air resistance of the model is ngeligibly small also at high speeds. The measurements are therefore purely hydrodynamical.

The preliminary tests were conducted with flat glass plates in order that the forward boundary line of the wetted surface might be determined. This boundary line under all speeds, loads, and trim angles had the shape of a very flat arc. In the subsequent tests there were therefore employed plates, some of aluminum and some of wood, glass strips being inserted at one-quarter width so that the mean value of the wetted length could be read off. In the case of very wide and V-bottom surfaces several glass strips were used.

The model was suspended without crowding so that all the errors in measuring the draft, trim, and longitudinal displacement of the model were negligibly small insofar as they were not eliminated by the calibration itself or by having the wires run on circular segments where required.

Pressure Distribution Measurement

For taking the pressure distribution measurements the planing surface was provided with about ninety measuring stations which were arranged in three longitudinal sections and a number of transverse sections. Figure 2 shows a measuring station in cross section. The free opening of the orifice is 2 millimeters in diameter. The glass tubes over the orifices are held fixed in position by means of a short pipe construction. In taking the measurement the planing surface is held fixed at the trim determined during the resistance measurements, the measurements being conducted with the water surface smooth. The heights of the water columns are marked. It was checked to see whether there was a possible interference effect of adjacent orifices by closing the orifices with plasticine in the check runs and keeping only one orifice open. No appreciable differences were observed. Check measurements with 1 millimeter free opening of the orifices showed, on account of the stronger throttling of the liquid columns, a smaller fluctuation.

For obtaining the pressure distribution it was necessary to make several test runs at each trim angle, slight speed differences which affected the loading on the adjusted plate being found unavoidable. The measuring accuracy is to be estimated at about ±5 percent of Δh.

THEORETICAL BASIS OF TESTS

For a surface in steady planing motion on a quiet frictionless fluid surface (fig. 3) the Bernoulli law may be applied to all the streamlines including the dividing streamline.

$$\frac{v^2}{2} + \frac{p}{\rho} + g\,z = \text{constant} \qquad (1)$$

The pressure p is assumed to be composed of the static pressure p_{stat} due to the weight of the fluid and the portion p_{dyn} due to the dynamic effects. The static lift is therefore

$$A_{stat} = \cos\alpha \int p_{stat}\, dF \qquad (2)$$

and for a flat rectangular planing surface may approximately be set equal to

$$A_{stat} = \gamma V = \gamma \frac{\alpha\, l^2\, b}{2} \qquad (3)$$

$(\sin\alpha = \alpha \quad \cos\alpha = 1 \quad \text{up to } 4°)$

if the wetted length l is determined during the test, it being assumed that the rise in level at the neighborhood of the planing surface is constant.

The dynamic lift is

$$A_{dyn} = \cos\alpha \int p_{dyn}\, dF \qquad (4)$$

and according to the momentum law is equal to the time rate of change of momentum of the mass of water involved

$$A_{dyn} = \frac{d\,(m\,v_o)}{dt} \qquad (5)$$

The total lift of the planing surface is thus

$$A = A_{stat} + A_{dyn} \qquad (6)$$

In the case of a viscous fluid the streamlines and velocities, in spite of the boundary layer occurring, agree approximately with those of the frictionless flow, differing only in the appearance of an additional tangential force T.

Owing to the effect of the finite width there is set up at the edges a cross flow with lateral pressure drop which for sufficiently large values leads to a separation of the water also at the side edges.

In the pure planing phase characterized by the separation of the water at the trailing and side edges of the planing surface the resistance of a flat surface as well as of all surfaces that are longitudinally straight and without twist is given by

$$W = W_N + W_R = A \tan \alpha + \frac{T}{\cos \alpha} \qquad (7)$$

The normal resistance

$$W_N = A \tan \alpha \qquad (8)$$

is proportional to the load and the trim angle but independent of the speed, while the frictional resistance

$$W_R = \frac{T}{\cos \alpha} \cong T = c_f' \, F \, q \qquad (8a)$$

is proportional to the wetted surface and the dynamic pressure, the friction coefficient c_f' being a function

of the Reynolds number $R = vl/\nu$ and depending on the nature of the boundary layer as well as on the roughness of the surface.

RESULTS OF THE TESTS AND APPLICATIONS

(A) The Flat Planing Surface

(1) Results of the Preliminary Tests with Flat Planing Surface

For the preliminary test on the flat rectangular planing surface average relations were chosen with regard to beam, load, and speed. Figure 4 shows a logarithmic plot of the beam at step b_{St} as a function of the flying boat weight G, or G/2 in the case of the twin-float seaplane, the load coefficient c_a' being taken as parameter. Selecting from the mean range a beam $b_{St} = 1.800$ meters and with $G = 5.185$ t and $c_a' = 0.889$, furthermore a mean airfoil lift $A = c_a F q = 1296$ kilograms,[1] independent of the trim angle and assuming a model scale $\lambda = 6$, then the model beam is $b_{St} = 0.300$ meter, the corresponding weight $G = 24$ kilograms and the hydrodynamic load at $v = 6$ meters per second — an average speed in the speed range in which the seaplane float executes a pure planing motion — $A^* = 18$ kilograms, then $c_B = 0.109$ and $F^* = 3.74$. The trim angle range of interest is $\alpha = 2^\circ$ to 10°.

Resistance, moment, center of pressure, and static lift.— On figure 5 are plotted the non-dimensional values ϵ, c_{mh}^*, l/b, l_p/l, and A_{stat}/A as functions of α. Tan α represents the lower limiting value of the resistance-load coefficient ϵ if according to equation (7) the frictional resistance W_R, on the assumption of frictionless fluid, becomes zero. Since with increasing trim angle α the ratio of the frictional

[1] $c_a = 1.2$ and $F = 80$ m² corresponding to 65 kg/m² surface loading.

portion of the resistance W_R to the total resistance W rapidly decreases on account of the strongly decreasing wetted area F, as may be seen from the trend of l/b, the ϵ curve approaches asymptotically the value tan α and for $\alpha > 10^\circ$ may be replaced approximately by tan α. Another asymptote is the axis of ordinates since F and hence W_R approach infinity as $\alpha \longrightarrow 0$. The position of the minimum lying between the asymptotes is determined by the ratio of the frictional to the total resistance. For average conditions this position lies between 4° and 6°.

Pressure distribution and character of flow.— Figure 6 shows the measured pressure distribution and the flow picture for the angles 4°, 6°, and 8°. The stagnation point lies near the leading edge of the wetted surface. The greatest portion of the water stream flowing up is thus deviated downward while the portion of the water lying ahead of the stagnation point is projected forward as spray. The maximum pressure, measured at the stagnation point remains considerably below the stagnation pressure. It is presumed that the full stagnation pressure occurs within so narrow a range that it does not show up in the measurement.

On account of the sharp-edge boundary of the planing surface the flow at the trailing edge already begins to separate at comparatively low speed and the water continues its downward motion behind the plate, thus forming a depression which is limited sideways by two wave trains coming from the side edges of the planing surface. The wave trains meet behind the planing surface in the plane of symmetry, and at the point of intersection the water spouts up in the manner of a fountain.

The transverse pressure drop produces a cross flow which for a sufficient speed leads to the separation of the water also at the side edges. The separation begins in the forward region of the pressure area even at the smaller speeds, on account of the relatively high pressure or pressure drop that occurs there, and with increasing speed continues toward the rear. The side spray rises steeply near the surface and then spreads out laterally.

Center of pressure.— If the trailing edge of the planing surface is chosen as the axis about which moments are taken the moments on the planing surface, according to figure 7 are

$$G\ l_1 + Z\ l_2 = N\ l_p = M_h\ St$$

Under the action of the applied moment at the left of the equation the planing surface trims to an angle α for which the hydrodynamic moment at the right is equal to the applied moment. A plot of the moment coefficient c_{mh}* shows the variation of the moment with the angle α. The greater the trim angle α the smaller is the increment $\Delta M_h\ St$ in the moment required to change the trim angle by an amount $\Delta\alpha$. The ratio

$$\frac{l_p}{l} = \frac{c_{mh}}{l/b\ c_a'} \qquad (9)$$

gives the position of the center of pressure if A is assumed to be approximately equal to N. According to the curve in figure 5 $l_p/l = 0.77$ with a tendency to decrease as the angle α decreases.

The moment of the static lift determined according to formula (3) is

$$M_{stat} = A_{stat}\ \frac{l}{3}\ \cos\alpha$$

so that the distance of the center of pressure is

$$l_p = \frac{M_{stat}}{A_{stat}} \cong \frac{l}{3} \text{ or } \frac{l_p}{l} = 0.333 \qquad (10)$$

The moment of the aerodynamic lift

$$M_{dyn} > A_{dyn}\ \frac{2}{3}\ l\ \cos\alpha$$

and the distance of the center of pressure

$$\frac{l_p}{l} > 0.666 \qquad (11)$$

if a triangular pressure distribution with the maximum lift at the leading edge is approximately assumed, since according to the measured pressure distribution the center of pressure lies always ahead of the center of pressure of a triangular pressure distribution the lever arm of which would be $2/3\ l \cos \alpha$.

From equations (10) and (11) the following may be said about the center of pressure travel: With increasing trim angle (A and v being constant) the ratio of static to total lift A_{stat}/A decreases and l_p/l increases, as is confirmed by the preliminary tests. With increasing speed (l/b and α constant) the dynamic lift increases with the dynamic pressure while the static lift remains constant. The ratio of the latter to the total lift therefore decreases and correspondingly l_p/l increases.

(2) Results of the Tests with Planing Surfaces

(a) Lift

The lift A by analogy with the similar expression used in aerodynamics may be expressed by the equation

$$A = c_a^* F q$$

In the case of the airfoil the lift coefficient c_a, in the middle range of the angle of attack and for small aspect ratios, is proportional to the angle of attack α and the derivative $dc_a/d\alpha$ = constant if l/b = constant. If, for the experimental range of angles, the same assumption is made for the planing surface (reference 7) then

$$c_a^* = \frac{dc_a^*}{d\alpha}\,\alpha = c_\alpha\,\alpha \qquad (12)$$

where the derivative is replaced by c_α. In order to eliminate α as parameter, as would be convenient for a suitable representation of the lift coefficient, it is therefore written

$$c_\alpha = \frac{A}{\alpha F q} \tag{13}$$

The test curves of figure 8 show that for the region of high Froude numbers F^* the assumption is sufficiently justified as a practical working hypothesis. Deviations from the straight line law may be ascribed to the gravity effect as will be further clarified below. If, in figure 9 c_α is plotted as a function of the aspect ratio l/b (reference 7), then from the foregoing considerations the Froude number F^* will be the parameter. The family of curves gives the results for all the lift coefficients obtained from the 33 test series indicated on the figure. To bring out more clearly the scattering of the points, since the plotting of all the test points would complicate the diagram, figure 9a shows the values for the test series 2, 14, and 22 to 33 with $F^* = 3.74$ the constant value. All values are well represented by the heavy averaging curve.

In figure 9b the lift coefficient values corresponding to the tests of Sambraus (reference 5) have been plotted. The wetted length l on the determination of which the accuracy of c_α mainly depends had to be obtained by photographic measurements in the Sambraus tests since the high speed carriage did not permit direct observation. Since the forward boundary of the pressure area at high dynamic pressures and small loads, such as were mostly assumed by Sambraus, fluctuated greatly even for an almost smooth water surface, (see Sec. II, 4 of reference 5) direct observations as made in the tests in the HSVA tank, in which the fluctuations may be well averaged, are more reliable. The scattering must be greater the shorter the wetted length — that is, the smaller the aspect ratio of the planing surface. Taking these conditions into consideration it is possible to speak of a reasonable agreement between the two series of tests with the exceptions of tests 2, 3, and 4 the coefficients of which are about 15 percent higher. The coefficients of the other test series of Sambraus lie 10 to 15 percent

higher only in the smallest aspect ratio range $l/b = 0.7$ to 1.2, agree for the medium aspect ratio range $l/b = 1.2$ to 2.5, and become somewhat less at the maximum aspect ratio $l/b = 3$.

In figure 9c there are similarly plotted the coefficients of the tests by Shoemaker (reference 6). In the American tests the wetted length was obtained by mirror observation of the spray coming off at the sides. This method, too, cannot lay claim to the same accuracy as the determination by direct observation of the forward contour of the pressure area through a glass strip inserted in the plate. Correspondingly, there is a considerable scattering of the values for small aspect ratios $l/b < 1$, the values lying on the average below those of the HSVA measurements so that in this range the latter values average approximately those of Sambraus and Shoemaker. At large aspect ratios the measurements agree very well since in this range an error in the determination of the wetted length only slightly affects the value of the lift coefficient.

For Froude numbers $F^* \geq 8.5$ the effect of gravity is negligibly small and the lift coefficient c_α is determined by the empirical equation

$$c_\alpha = 0.845 \left(\frac{l}{b}\right)^{-1/2} \qquad (14)$$

In the previous section it was established that the fraction of the static displacement increases with decreasing trim angle or increasing aspect ratio. The curves with different F^* parameter therefore diverge in the direction in increasing l/b.

As a limit of the pure planing condition — that is, when the sides of the planing surface begin to be wetted at the step — there is obtained a straight line passing through the family of curves

$$c_\alpha = 0.94 \left(\frac{l}{b}\right)^{-0.375} \qquad \left(\text{if } \frac{l}{b} \geq 0.75\right) \qquad (15)$$

which at the same time connects the minimums of the curves.

Comparison with the flat plate in an air stream.- The wind tunnel tests carried out by Winter (reference 8) on flat plates of various aspect ratios provide a means of comparison between the planing surface and an airfoil. In the table are given the coefficients of the total lift coefficient in the air $c_{\alpha\,tot} = \frac{c_N \cos \alpha}{\alpha}$ as a function of l/b for $\alpha = 10^\circ$. From the pressure measurement (fig. 23 in Winter's paper) there is obtained by integration, for $\alpha = 9.5^\circ$ of the pressure distribution on the top and bottom sides, the ratio of lift on the two sides $A_{bot}/A_{top} = \frac{0.39}{0.61}$ or

$$A_{bot} = 0.39\ A_{tot} \tag{16}$$

If for the angle-of-attack range considered the above relation in the absence of pressure distribution measurement at small angles of attack is assumed constant with change in angle of attack and aspect ratio, then the straight line in figure 9b

$$c_\alpha = 0.91 \left(\frac{l}{b}\right)^{-1/2} \tag{17}$$

gives the change in the lift coefficient on the bottom side of the flat rectangular plate in air. Formulas (14) and (17) differ only by the value of the constant and that to such a small extent that the lift coefficients in air and water may be said to agree as long as the effect of gravity is negligible.

Flat Rectangular Plate in Air

$F = 0.500\ m^2$, $v = 28\ m/s$, $\alpha = 10^\circ$

l/b	c_N	$c_{\alpha_{tot}}$	$c_{\alpha_{bot}}$
0.5	0.576	3.25	1.27
.666	.520	2.93	1.14
.80	.468	2.64	1.03
1.0	.412	2.32	.905
1.517	.338	1.91	.745
2	.300	1.69	.66
2.86	.237	1.34	.522
7.48	.155	.875	.341

Comparison with the theory of Wagner and the results of Sambraus.— On figure 9b is plotted the lift coefficient c_α according to the Wagner theory for the short plate. The curve, which was obtained by neglecting gravity, is to be compared with the curve from formula (14) for which the effect of gravity is negligibly small. In the range of small aspect ratios the theoretical curve lies about 20 percent above that obtained from the test results where, however, it is to be noted that in the theory, on the assumption of infinitely small angle of attack A_{bot} has been set equal to $0.5\ A_{tot}$; whereas, for finite angles of attack the pressure measurements of Winter give the ratio of formula (16). A complete agreement between test and theory is therefore not to be expected. In the neighborhood of $l/b = 2$ the curves intersect and diverge with increasing aspect ratio.

In the case of long planing surfaces ($l/b \gtrsim 3$) there is good experimental agreement with the flat airfoil in air (under the assumption $c_{\alpha_{bot}} = 0.39\ c_{\alpha_{tot}}$); whereas the Wagner theory of the short plate does not agree with the test results also for planing conditions for which the effect of the earth's gravity is negligible. (The theory of the long plate gives greater deviations from the experimental results as shown by Sambraus.)

The conclusions of Sambraus on the long flat planing surface (Summary points 1 to 3 in reference 5) thus find no confirmation while point 4 is to be supplemented by the statement that at high Froude numbers F^*[1] the lift in the investigated range at constant aspect ratio varies linearly with the trim angle but that with decreasing Froude number the lift coefficient as a result of the increasing, favorable, effect of gravity increases so that d_{ca}^*/d_α does not remain constant.

(b) Resistance

From formula (8a) there is obtained for the frictional coefficient $c_f' = W_R/F\,q$. When plotting c_f' as a function of the Reynolds number $R = v\,l/\nu$ and comparing with the results of pure friction measurements, the following points are to be noted:

1. The normal resistance W_R^N obtained by subtracting from the measured total resistance W is, in the range of minimum resistance of about the same magnitude, and for higher trim angles, considerably larger than the frictional resistance W_R. Since the scattering contribution of the measurement on W_R is removed, the scattering of c_f' must be relatively large and increases with increasing trim angle.

[1] In the presentation here chosen the Froude number $F^* = v/\sqrt{g\,(\Delta/\gamma)^{1/3}}$ is proportional to the speed and inversely proportional to the square root of a dimension which increases with increasing lift; namely, the length of an edge of the water cube in correspondence with the physical interpretation of the Froude number. The number chosen by Sambraus $F = v/\sqrt{g\,b}$, which fulfills its purpose as regards considerations of similarity, increases, however, with decreasing width b, also, for example, when the wetted length remains constant with decreasing load. This representation is not suitable for the work under consideration. If the F^* number (see fig. 9b) is used for the Sambraus tests, it appears that the latter only slightly exceed the F^* range of our own tests in spite of higher test speeds on account of the application of narrower plates.

2. The scattering is increased by the fact that the measured value of the wetted surface F fluctuates more the smaller the value of l – that is the larger the angle α.

3. The water thrown up in front as spray partially wets the bottom surface and decreases the resistance (reference 4). This thrust cannot be determined and is thus not taken into account.

4. The total pressure surface is used in the computation as the wetted surface in spite of the fact that the direction of motion of the water particles at the surface ahead of the stagnation line is forward and in the side regions has a side component.

5. The high pressure region is superposed on the frictional boundary layer with the result of a decrease in speed so that $v_m < v$. This decrease in speed is not taken into account.

6. The Reynolds law assumes geometrical similarity of the flow. This requirement is not satisfied since it is possible that the wetted length l and hence also R may be constant for various loads; whereas the trim angle and hence the pressure and velocity distribution are different.

In figure 10 are plotted the curves for the series of tests 1 to 33. It may be seen that in spite of the above restrictions the values of c_f' are relatively well represented by the curve given by Prandtl (reference 9) for the turbulent boundary layer with preceding laminar layer.

$$c_f = \frac{0.455}{(\log R)^{2.58}} - 1700/R \qquad (18)$$

if it is taken into account that the scattering that underlies the Prandtl curve is likewise not small.

The measurements were partly conducted in completely quiet water: namely at the beginning of the tests and after long intervals and partly in water with a slight amount of motion. The relatively small scattering is therefore a proof of the fact that in each case only a

single stable form of the boundary layer exists. This is of particular importance for the model test since the larger portion of the towing test occurs within the range of Reynolds numbers in which there might possibly have been two boundary layer conditions and hence fluctuations in the frictional resistances up to about 100 percent.

For Reynolds number $R < 10^6$ the surface tension at mean pressures

$$p_m = \frac{A}{l\ b} < 20 - 50\ kg/m^2 \qquad (19)$$

results in the wetting of the sides of the planing surface, thereby producing a considerable increase in the resistance. Under these conditions spray no longer occurs. The condition for the occurrence of the pure planing process is therefore, according to formula (15), $c_\alpha < 0.94 \left(\frac{l}{b}\right)^{-0.375}$ and, according to formula (19), $p_m > 20 - 50\ kg/m^2$. In the towing test, for considerable intervals during the take-off process, $p_m < 20-50\ kg/m^2$ if the scale of the model is made too small; then the model results are no longer transferable to full scale. The test series 31 to 33 belonging to a single scale series lie in this range and partly also in the test series 10 and 11, for which reason in the latter case the c_f' values rise unsteadily with decreasing mean pressure (increasing l and R). That these values of c_f' lie in the range of the curve for turbulent boundary layer is physically not justified and may be considered as an accidental result.

(c) Center of Pressure

The fundamental observations previously made on the effect of the earth's gravity on the position of the center of pressure are confirmed in the family of curves (fig. 11) which shows l_p/l as a function of l/b with the Froude number F^* as parameter. For Froude numbers greater than 8 $l_p/l = 0.8$ constant. Both with decreasing F^* and with increasing aspect ratio (if $F^* < 8$) the center of pressure moves in the direction of the trailing edge of the planing surface.

(3) Application of the Results to the Determination of the Effect of the Beam, Load, Speed, and Scale in the Range of Pure Planing

In the following paragraphs a number of illustrative examples will be computed as regards lift, resistance, and center of pressure and thereby a number of important questions with regard to the planing problem will be clarified. In the following diagrams therefore in addition to the numerically computed curves there will also be indicated the test points obtained from measurement so that the extent of agreement of the families of curves in the working charts will become clear.

There will first be described the procedure for the numerical computation. Let there be given the width b of a flat rectangular planing surface, the lift A, and the planing speed v and hence also the Froude number $F^* = v/\sqrt{g\,(A/\gamma)^{1/3}}$. It is required to find the resistance-load ratio ratio ϵ and the moment coefficient $c_{mh}{}^*$ as functions of the trim angle α. Corresponding to a number of suitably chosen l/b values there are determined from figure 9 for the parameter F^* the lift coefficient c_α. From the equation

$$\text{arc } \alpha = \frac{A}{c_\alpha \; l/b \; b^2 \; q}$$

there is obtained the trim angle α. The Reynolds number is

$$R = \frac{v}{\nu} \; \frac{l}{b} \; b$$

The corresponding frictional coefficient $c_f{}'$ is taken from figure 10, the curve for turbulent boundary layer with preceding laminar layer and

$$\epsilon_R = \frac{W_R}{A} = c_f{}' \; \frac{l}{b} \; \frac{b^2}{A} \; q$$

is determined. Therefore

$$\epsilon = \epsilon_R + \tan \alpha$$

Further, for the intersection point of the c_α curve and the limiting curve of pure planing in figure 9 there are determined the corresponding aspect ratio and limiting angle, respectively, at which the character of the flow changes. The dotted portions of the illustration curves apply to conditions for which the pure planing process has not yet been reached so that it may be expected that the measurement results exceed the computed results on account of additional resistances.

From figure 11 l_p/l is similarly determined and with $H_{h\,St} \cong l_p\,A$

$$c_{mh}{}^* = \frac{M_{h\,St}}{A\,(A/\gamma)^{1/3}} = \frac{l_p}{l}\,\frac{l}{b}\,\frac{b}{(A/\gamma)^{1/3}}$$

(a) Effect of the Width

For the interpretation of the test results on floats it is of importance to determine how the resistance-load ratio and moment coefficient vary with the width for constant load and planing speed.

Five flat rectangular planing surfaces of various widths, in comparison with the initial test with planing surface A, were investigated according to the following test schedule:

Planing surface	Test number	b_m	A_{kg}	c_B	$v_{m/s}$	F^*
1	22	0.600	18	0.0272	6	3.74
2	23	.500	18	.0392	6	3.74
11	24	.400	18	.0612	6	3.74
A	2+25	.300	18	.1090	6	3.74
3	26	.225	18	.1940	6	3.74
4	27	.150	18	.4350	6	3.74

In figure 12 the resistance and moment coefficient ϵ and $c_{mh}{}^*$ computed from the measured values have been plotted as functions of α with b as parameter.

the continuous curves giving the coefficients determined by computation. The example shows that in the case of the flat plate for which the full width contributes to the lift the optimum resistance—load ratio becomes continuously more favorable with increasing width and decreasing aspect ratio or wetted area.

In the range of small widths the impairment of the ratio due to the increasing effect of gravity decreases. If the pure planing process discontinues, however, the ratios again increase on account of the additional edge resistances.

As limiting value of the width at the steps of sea floats there is given in figure 4 for the wide float the value $b_{gt} = 1.4\ (G/\gamma)^{1/3}$ and for the narrow float $b_{gt} = 0.7\ (G/\gamma)^{1/3}$. If for the tests under consideration, according to the assumptions of the preliminary test, the displaced weight at rest is chosen as $G = 24$ kilograms, then the beams corresponding to the beam at the step in the model are $b_{large} = 0.4$ meter and $b_{small} = 0.2$ meter. For these values there are obtained the optimum load—resistance ratios of 0.122 and 0.154, the difference amounting to 26 percent.

The effect of the beam on the trim angle becomes clear if the angle is determined as a function of the beam for constant c_{mh}*. For the previously mentioned limiting beams there is obtained a difference of about 5 percent.

The beam of the planing surface has a great effect on the intensity of the spray. Since the lift coefficient decreases with decreasing aspect ratio; that is, with increasing beam, there is a reduction in the displaced volume of water and in the wetted side length, at which the spray escapes. The extent by which the spray formation may differ in the two previously defined limiting beams may be seen from figure 13 where the two models are equally loaded and have the same speed and trim angle. Figure 14 shows, for the example given, the ratio of the static displacement V to the total lift $V\ \gamma/A$ as a function of α and it may be seen that for the two limiting cases the displaced volume of water of the narrow float exceeds that of double the beam by 5 to 10 times.

In this connection the position of the depression behind the planing surface is also of significance. In the first and second portions of the take-off process of a seaplane the stern lies behind the fountain on the water thus relieving the load on the forebody and, on account of the small initial trim of the float, resulting in a negative trim by the stern, there is even set up a thrust that lowers the resistance (reference 2).

The distance c of the fountain behind the trailing edge was measured in tests 22 to 27 as well as in a special test with planing surface A using a load corresponding to the take-off process. In figure 15 the values $l + c$ are plotted against the trim angle α. It may be seen that $l + c$ is practically independent of α so that the position of the fountain with change in trim angle is shifted in the same sense as the contour of the wetted surface. The value of $l + c$ is approximately proportional to F^* and b

$$l + c = 1.8 F^* b \qquad (20)$$

as may be derived from figure 15[1].

(b) Effect of Load

It will now be determined how, for a given beam and speed, the resistance-load ratio and the moment coefficient vary with the load.

For constant speed and a large range of loads, tests were conducted on planing surface A according to the following test schedule:

Planing surface	Test number	b_m	A_{kg}	c_B	v_m/s	F^*
A	18	0.3	10	0.0218	10	6.90
A	19	.3	25	.0545	10	5.90
A	16	.3	50	.109	10	5.26
A	20	.3	100	.218	10	4.70
A	21	.3	150	.327	10	4.38

[1]As expression given by Weinig (reference 12) of the fountain distance does not agree with the results obtained by the author and not published at the time and is therefore not taken into account here.

In figure 16 the measured values ϵ and c_{mh} are plotted against α with c_y as parameter and the theoretically computed curves are also shown. It may be seen that for small and average loads the resistance-load ratio increases considerably with increasing load on account of the impairment of the aspect ratio. In doubling the load, for example, from 25 to 50 kilograms, ϵ_{opt} increases by 25 percent. At very large loads the impairment is slight on account of the increasing effect of gravity.

Check of the relation d_{ca}^*/d_α = constant in the investigated range for higher F^* numbers.- In figure 8 for tests 16, 18, and 19 the wetted lengths l have been plotted against α and made to intersect the straight lines l = 0.3, 0.6, and 0.9 meter, corresponding to the aspect ratios l/b = 1, 2, 3. The c_a^* values are also plotted. These lie on straight lines which pass through the origin - that is, in the range of F^* numbers, within which the effect of gravity may be entirely or approximately neglected d_{ca}^*/d_α = constant and thus the assumption underlying formula (12) is justified.

(c) Effect of the Speed

The take-off diagram of a seaplane shows two resistance maximums, the first in the range of the transition from the floating to the planing condition, the second before the get-away. It will now be investigated to what extent the formation of these maximums depend on the stern of the float. This question may be answered with the aid of the planing surface which is equivalent to the longitudinally straight forebody.

For a larger speed range with constant beam and load the resistance and moment coefficients were computed, the tabulated results being given as follow:

Planing surface	b_m	A_{kg}	c_B	v_m/s	F^*	F
A	0.3	50	0.436	5	2.63	2.93
A	.3	50	.302	6	3.16	3.50
A	.3	50	.222	7	3.69	4.09
A	.3	50	.170	8	4.21	4.67
A	.3	50	.134	9	4.74	5.28
A	.3	50	.109	10	5.26	5.84
A	.3	50	.0757	12	6.32	7.00
A	.3	50	.0556	14	7.38	8.18
A	.3	50	.0424	16	8.44	9.35

Plotting ϵ and c_{mh} as functions of α with v as parameter, figure 17, there is found the type of relation familiar from float investigations. At low speeds ϵ increases approximately linearly with α, the pure planing process not yet occurring. With increasing speed the resistance increases, particularly so at small trim angles so that a maximum resistance is soon obtained at moderate trim angles. After exceeding the maximum the resistance again decreases with increasing speed. A second maximum therefore does not appear in the case of the planing surface and the appearance of such a maximum for the float is to be ascribed to the wetting of the stern by the spray. In the plot, figure 18, giving ϵ and c_{mh} as functions of F the formation of the first maximum is brought out with particular clearness. The indicated boundary curve of the pure planing condition shows that the latter occurs before the maximum is reached. Resistance and moment maximums lie, as also in the case of float investigations, at about the same speeds, so that the greatest trim angle coincides with the resistance maximum if the planing surface planes free to trim.

Whereas, with decreased speed the resistance-load ratio increases on account of the impairment of the aspect ratio and on neglecting gravity there would be obtained the upper curve of figure 19, the effect of gravity in the lower speed range is to decrease the resistance to such an extent that with the second curve branch a resistance maximum occurs. By support of the stern the maximum in a float may be considerably affected as explained in reference 2.

(d) Effect of the Scale

It will now be investigated to what extent similarity applies as regards the pressure surfaces and center-of-pressure position and whether the scale effect is given solely by the dependence of the frictional coefficient on the Reynolds number. By investigating a family of planing surfaces this question may be answered for the case of the pure planing process.

Six plane rectangular planing surfaces of various beams were investigated according to the following test schedule:

Planing surface	Test number	Full-scale flying boat λ_F	Full-scale twin float seaplane λ_S	b_m	c_B	A_{kg}	F^*	v_m/s
		1		2.400	0.109	9216	3,74	16.96
		2	1	1.200	.109	1152	3.74	12
1	28	4	2	0.600	.109	144	3.74	8.48
2	2, 25, 29	8	4	.300	.109	18	3.74	6.00
3	30	10.66	5.33	.225	.109	7.6	3.74	5.20
4	31	16	8	.150	.109	2.25	3.74	4.24
5	32	24	12	.100	.109	.660	3.74	3.46
6	33	32	16	.075	.109	.281	3.74	3.00

In figure 20 the values of ϵ, l/b, and $c_{mh}{}^*$ obtained from the measured values are plotted against α with λ_F as parameter. Planing surface 1 within $b = 0.600$ meter is the widest of all surfaces investigated. For the scale comparison the full-scale design was a flying boat of beam $b = 2.400$ meters with $A = 9216$ kilograms and $G = 12,288$ kilograms ($\lambda_F = 1$). The planing surface with $b = 1.200$ meters and $A = 1152$ kilograms, $G = 1536 \times 2 = 3072$ kilograms corresponds to the design of a normal twin-float seaplane ($\lambda_S = 1$).

The continuous curves show the variation of the values obtained by computation which were determined for all conditions for which $p_m > 50$ kg/m^2. At smaller pressures at which, on account of the effect of surface tension, the pure planing process has discontinued the determination of the resistance is not possible. In this case the dotted curves show the variation in the measured values.

The values determined in the series of tests for the aspect ratio l/b and the moment coefficient c_{mh}* arrange themselves in such a manner that no regular deviation from an averaging curve through the test points (this curve has not been drawn on the diagram) can be established — that is, in the pure planing process there is complete similarity of wetted surface and moments and hence also of pressure distribution. The similarity still holds in those ranges in which the surface tension exerts an effect on the planing condition.

The resistance-load ratios become more favorable with increasing size of planing surface on account of the decreasing resistance coefficient, a shift in α_{opt} toward small angles taking place. On account of the fact that c_f' is approximately constant in the range $R = 1 \div 5 \times 10^6$ the ratios are practically equal for average scales. With further decrease the resistances strongly increase on account of the effect of the surface tension, with α_{opt} shifting considerably in the direction of higher angles.

The impairment in ϵ for equal c_{mh}*, l/b, and α for the flying boat and twin float seaplane is given in the following table:

Flying boat b = 2.400 m		Twin float seaplane b = 1.200 m	
λ_F	percent	λ_S	percent
2	7.2	2	3.8
4	11.3	4	10.5
8	18.5	5.33	21.8
10.66	30.6	8	32.3
16	42	12	77.4
24	90	16	107
32	122		

The above figures show that tests with models of too small a scale ($b < 0.15$ m) such as were mainly conducted in England, for example, (reference 10) and in Italy, (reference 11) since the beginning of float investigations, cannot be used for the determination of the resistance, since the additional resistances arising under the effect of the surface tension cannot be determined. Also in the case of somewhat larger models the difference in the ratios between model and full-scale design is still considerable. A transfer of the model test results according to the method here given to the full-scale design is practically impossible on account of the difficulty during the test in determining the wetted area by measurement. It is only after the construction of towing tanks with high carriage velocities that tests on large scale models became possible for which, even with no account being taken of the scale effect — that is, with the assumption:

$$W = w\,\lambda^3 \quad \text{or} \quad \epsilon_H = \epsilon_M$$

and

$$H = m\,\lambda^4 \quad \text{or} \quad c_{mh_H} = c_{mh_M} \qquad (21)$$

results are obtained that deviated from the true values only within the accuracy usual in passing from the model to full-scale computations.

The above example shows that in passing from the model to the full-scale design according to formula (21) one is on the safe side. On account of the additional roughness and wave effect (reference 13) which occurs particularly in the case of riveted sheet bottom of the full-scale design the actual differences between the resistance computed from the model and the true one are smaller than given in the previous table as is shown by scale tests conducted on families of floats (references 14 and 15).[1]

---

[1]The possibility should be noted that in the model of very large scale the difference of the friction coefficient of the model and full-scale design is so small that on account of the roughness and wave effect the resistance of the full-scale design may be higher than that obtained from the model computation but does not come into consideration in the case of the usual scales employed.

(B) The V-Bottom Planing Surface

(1) Basic Equations and Determination of the Lift, Resistance, and Center of Pressure

For a longitudinally straight V-bottom planing surface the resultant normal force on one side is according to figure 21

$$\frac{N}{2} = \frac{A}{2 \cos \vartheta}$$

or the total normal force

$$N = \frac{A}{\cos \vartheta} \qquad (22)$$

The lateral components Q balance out.

The production of the lateral speeds corresponding to the lateral components Q for equal lift and otherwise equal conditions, particularly equal effective beam results in an additional exit loss and hence an increased resistance which corresponds approximately to an increase in the load and is equivalent to a lift increase from A to $N = A/\cos \vartheta$. That this actually represents a useful approximation is also shown by the analysis of the further tests. There is therefore set

$$c_a = \frac{N}{\alpha F_D q} = \frac{A}{\cos \vartheta \, \alpha F_D q} \qquad (23)$$

For the length there is taken the mean length l_m of the wedge-shape surface F_D the forward bounding line of the pressure area, in correspondence to test measurements being taken as a straight line, and a stagnation of constant height along this line being assumed. The aspect ratio is then

$$\frac{l}{b} \equiv \frac{l_m}{b} \equiv \frac{l_m}{b_{nat}} \tag{24}$$

From figure 22 the length of the pressure area at the keel, equal to the maximum wetted length, is determined by

$$l = l_m + \frac{b}{4}\frac{\tan \vartheta}{\tan \alpha} \tag{25}$$

and at the outer edge of the planing surface

$$l_a = l_m - \frac{b}{4}\frac{\tan \vartheta}{\tan \alpha}$$

The full beam of the V-bottom planing surface contributes to the support as long as

$$l_a \geqq 0$$

or

$$\frac{l_m}{b} - \frac{\tan \vartheta}{4 \tan \alpha} \geqq 0$$

and therefore

$$\frac{l_m}{b} \geqq \frac{\tan \vartheta}{4 \tan \alpha} \tag{26}$$

If

$$\frac{\tan \vartheta}{4 \tan \alpha} > \frac{l_m}{b}$$

the natural beam b_{nat} of the pressure surface is below that of the beam b of the planing surface and

$$\frac{l_m}{b_{nat}} = \frac{\tan \vartheta}{4 \tan \alpha} \tag{27}$$

In contrast to the flat surface for which, with increased beam of the planing surface the aspect ratio of the pressure area also becomes more favorable, since the trailing edge of the planing surface is always utilized to its

full extent, in the case of the V-bottom surface there occurs a limiting beam b_{nat} of the pressure area which is at the same time the most favorable beam of the planing surface for the given load relations. The portions of the planing surface lying outside of the pressure area are wetted by the spray which is retarded on the surface and so increases the resistance. They are therefore, without being utilized for the support of the surface, the cause of additional resistances which are larger the more the width of the planing surface exceeds the natural width of the pressure area.

In the case of the seaplane float this condition occurs according to figure 23 before the get-away. Since in the outer free bottom strip of width $(b - b_{nat})$ a powerful spray is directed backward, the stern of one float is also wetted and under certain conditions such large additional resistance may be set up that in spite of the small residual loading of planing bottom the total resistance of the aircraft attains the value of the propeller thrust and take-off is impossible.

The assumptions required for the numerical determination of the friction coefficient on the size of the wetted surface F and the Reynolds number R obtained on the basis of test observations are the following figure 23a.

Case 1) loaded beam: b if $\frac{\tan \vartheta}{4 \tan \alpha} < \frac{l_m}{b}$

Case 2) loaded beam: $b = b_{nat}$ if $\frac{\tan \vartheta}{4 \tan \alpha} = \frac{l_m}{b}$

$$F = \frac{l\, b}{\cos \vartheta}$$

$$R = \nu \frac{l}{b} \frac{b}{\nu}, \quad \text{where} \quad \frac{l}{b} = \frac{l_m}{b} + \frac{\tan \vartheta}{4 \tan \alpha} \qquad (28)$$

Case 3) loaded beam: b_{nat} if $\frac{\tan \vartheta}{4 \tan \alpha} > \frac{l_m}{b}$

and $\tan \gamma = \frac{2\, l}{l - b_{nat}} \geqq 10$

There is then obtained

$$b_{nat} = \sqrt{\frac{A}{c_\alpha \cos \phi \frac{l_m}{b_{nat}} q \alpha}}$$

and

$$l = 2 \frac{l_m}{b_{nat}} b_{nat}$$

so that

$$\left.\begin{aligned} F &= \frac{l (b + b_{nat})}{2 \cos \phi} \\ R &= \frac{v l}{\nu} \end{aligned}\right\} \qquad (29)$$

Case 4) loaded beam: b_{nat} if $\frac{\tan \phi}{4 \tan \alpha} > \frac{l_m}{b}$

and $\tan \gamma = \frac{2 l}{b - b_{nat}} < 10$

$$\left.\begin{aligned} F &= \frac{l \left(b_{nat} + \frac{l}{10}\right)}{\cos \phi} \\ R &= \frac{v l}{\nu} \end{aligned}\right\} \qquad (30)$$

In cases 1 and 2 the water escaping from the forward contour of the wetted surface and the water running along the surface as a film covers almost the entire width of the surface so that l is to be used in the determination of F and R. In case 3 the limit of the spray water wetting is given approximately by the dotted curve. In case 4 no further wetting of the edge portions occurs with further increase in width of the planing surface. The limiting value is for $\tan \gamma = 10$.

(2) Application of the Results for the Determination of:

(a) The Effect of the V angle

Whereas, the impact forces in take-off and landing decrease with increase in V angle of the float, the resistance increases. The dependence of the resistance on the V angle will now be found.

Four rectangular planing surfaces of various V angles and constant beam were investigated according to the following test schedule

Planing surface	Test number	ζ	A_{kg}	c_B	v_m/s	F^*
A	2 & 25	180°	18	0.109	6	3.74
7	34	160°	18	.109	6	3.74
8	35	150°	18	.109	6	3.74
9	36	132°	18	.109	6	3.74
10	37	100°	18	.109	6	3.74

In figure 24 the computed coefficients ϵ and c_{mh}^* are plotted against α with ζ as parameter; the values of c_{mh}^* being given by the dotted curves. The computed curves are continuous. Very good agreement is shown between the computed and test values of ϵ, the assumption lying at the basis of formula (23) thus being confirmed. Only in the case of the sharpest V bottom do the test values at small trim angles show any deviation from the general shape of the curves since in this case the statically displaced volume of water is practically equal to the entire lift so that in spite of free side edges the process is more like that of floating than that of planing. Correspondingly the pressure drop at the sides is small and hence the spray formation weak. The depression is strongly keeled and there is formed a short distance behind the planing surface a low fountain extending over some distance. The spray development then increases up to a V angle of between 100° and 132°. With further increase in the angle, however, there is a strong decrease in the spray.

The angle of minimum resistance α_{opt} increases with increasing V angle. The connecting-straight line α_{opt} has according to the assumption made in the computation the same trend as on increasing the load of a flat surface (fig. 16). For α_{opt} according to figure 24 there is an increase in the drag with V angle given by

$$\frac{\epsilon - \epsilon_o}{\epsilon_o} 100 = 1 + 40\vartheta + 82\vartheta^2 \qquad (31)$$

In the formula for the flat plate if l is replaced by l_m there is obtained

$$c_{mh}{}^* = \frac{l_p}{l_m} \frac{l_m}{b} \frac{b}{(A/Y)^{1/3}}$$

The agreement of the computed and experimentally determined values of $c_{mh}{}^*$ is very good up to medium V angles; at larger angles for constant $c_{mh}{}^*$ the difference remains less than 1° so that here too a sufficiently accurate determination of the trim angle is possible.

(b) Effect of the Beam

In the take-off of a seaplane the width of step of the V-bottom float, on account of the small residual load and the high dynamic pressure exceeds the natural width of the bottom surface under pressure, in contrast to the flat bottom for which the full beam at step in the pressure area is utilized. The most favorable width of the V bottom depends therefore on the load and the dynamic pressure.

For the purpose of testing these conclusions planing surfaces with two V-bottom angles and various beams were tested according to the following test schedule:

Planing surface	Test number	ζ	b_m	A_{kg}	c_B	c_B^*	v_m/s	F^*
12	38	150°	0.150	18	0.435	0.142	6	3.74
13	35	150°	.30	18	.109	.142	6	3.74
14	39	150°	.472	18	.044	.142	6	3.74
15	40	150°	.772	18	.0164	.142	6	3.74
12	43	150°	.150	50	.435	.071	10	5.26
13	44	150°	.300	50	.109	.071	10	5.26
14	45	150°	.477	50	.0431	.071	10	5.26
15	46	150°	.772	50	.164	.071	10	5.26
17	36	132°	.300	18	.109	.142	6	3.74
18	41	132°	.444	18	.0498	.142	6	3.74
19	42	132°	.730	18	.0184	.142	6	3.74
16	47	132°	.150	50	.435	.071	10	5.26
17	48	132°	.300	50	.109	.071	10	5.26
18	49	132°	.444	50	.0431	.071	10	5.26
19	50	132°	.730	50	.0164	.071	10	5.26

In figures 25 to 28 the measured values of ϵ are connected by dotted curves and c_{mh}^* plotted against α. The continuous curves give the results of the computed values. The differences between the two are indicated by arrows. Since beyond the limiting curve, (fig. 9) no pure planing condition is set up, the computed curves are also dotted. Good agreement is obtained between the planing process determined from the diagram and that from the observed appearance of the free planing condition.

In a comparison of the values of ϵ for pure planing conditions it is found that the test values are always somewhat below the computed values but otherwise the curves are similar. This is probably to be ascribed to the fact that the mean flow direction on the additional wetted areas does not agree with the direction of travel so that the resistance is increased only by a component of the additional frictional resistance. In spite of this for most purposes the numerically computed values are sufficient (greatest difference $\Delta\epsilon = 0.025$).

An optimum beam which is obtained both experimentally and by computation in the above example lies between the two mean beams, the experimental value being somewhat higher than the computed value.

The values of c_{mh}* agree very well, the differences between experiment and computation amounting for constant c_{mh}* mostly to less than $1/2^{\circ}$ and in the most unfavorable case to less than 1°.

Translation by S. Reiss,
National Advisory Committee
for Aeronautics.

REFERENCES

1. Baker, G. S., and Millar, G. H.: Some Experiments in Connection with the Design of Floats for Hydro-Aeroplanes. R. & M. No. 70, British A.R.C., 1912.

2. Sottorf, W.: The Design of Floats. NACA TM No. 860, 1938.

3. Sottorf, W.: Experiments with Planing Surfaces. NACA TM No. 739, 1934.

4. Wagner: Über das Gleiten von Wasserfahrzeugen. Jahrbuch STG 1932. Über das Gleiten von Körpern auf der Wasseroberfläche. Proc. Fourth Int. Cong. for Appl. Mechanics. Cambridge, 1934.

5. Sambraus, A.: Gleitflächenversuche bei hohen Froudeschen Zahlen. Luftfahrtforschung. Bd. 13, June 20, 1936, pp. 190–198.

6. Shoemaker, James M.: Tank Tests of Flat and V-bottom Planing Surfaces. NACA TN No. 509, 1934.

7. Perring, W. G. A., and Johnston, L.: The Hydrodynamic Forces and Moments on Simple Planing Surfaces, and an Analysis of the Hydrodynamic Forces and Moments on a Flying Boat Hull. R. & M. No. 1646, British A.R.C., 1935.

8. Wintor: Strömungsvorgänge and Platten und Profilierten Körpern bei kleinen Spannweiten. VDI-Forschung, nos. 1 and 2, 1935.

9. Prandtl, L.: Zur Turbulenten Strömung in Rohren und längs Platten. Ergebnisse der Aerodynamischen Versuchsanstalt zu Göttingen. IV. Lfg., 1932. pp. 18–29.

10. Gouge, A.: The Design of Seaplanes. Aircraft Engineering, Aug. 1930, pp. 202–206.

11. Eula, Antonio: Hydrodynamic Tests of Models of Seaplane Floats. NACA TM No. 770, 1935.

12. Weinig: Erörterungen zu Wagner.

13. Kempf: Über den Einfluss der Rauhigkeit auf den Widerstand von Schiffen. Jahrbuch STG 1936.

14. Sottorf, W.: Scale Effect of Model in Seaplane-Float Investigations. NACA TM No. 704, 1933.

15. Schmidt, Rudolph: The Scale Effect in Towing Tests with Airplane-Float Systems. NACA TM No. 826, 1937.

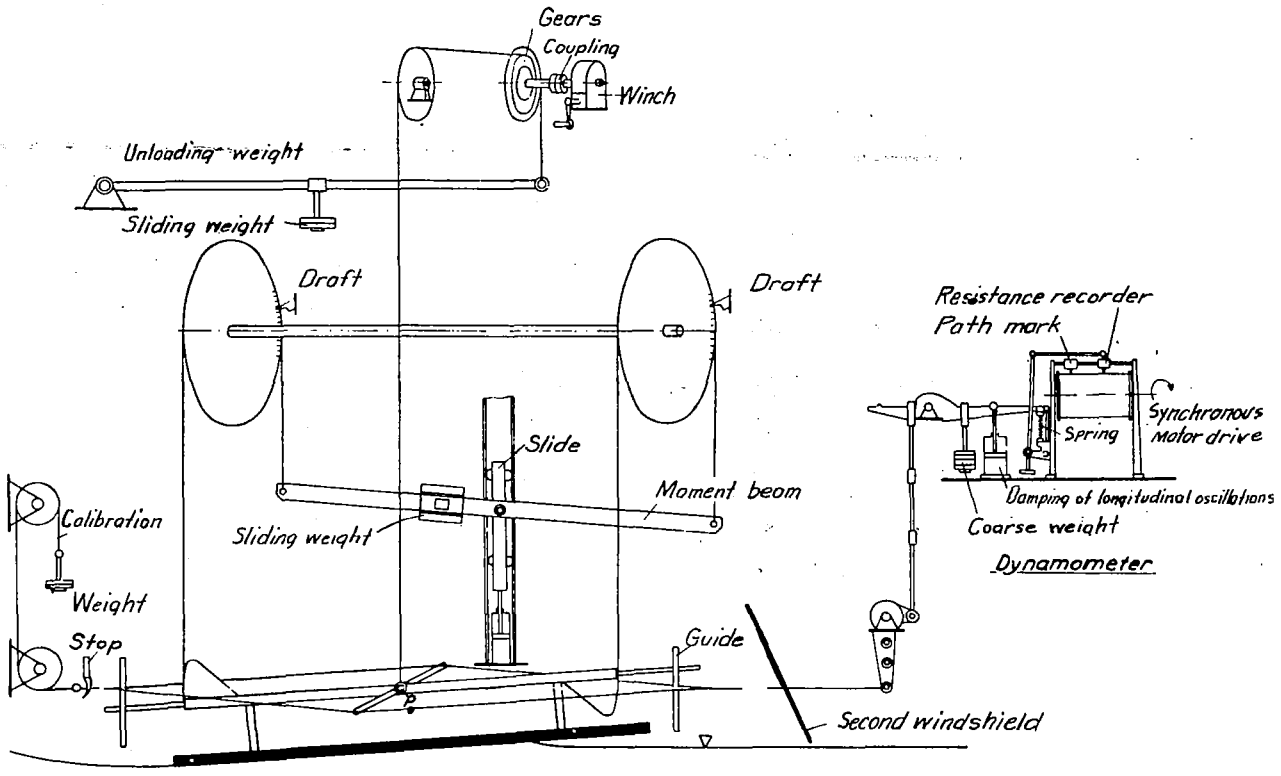

Figure 1.- Set-up of measuring apparatus.

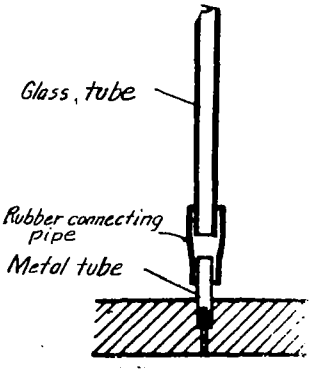

Figure 2.- Cross section of a pressure orifice.

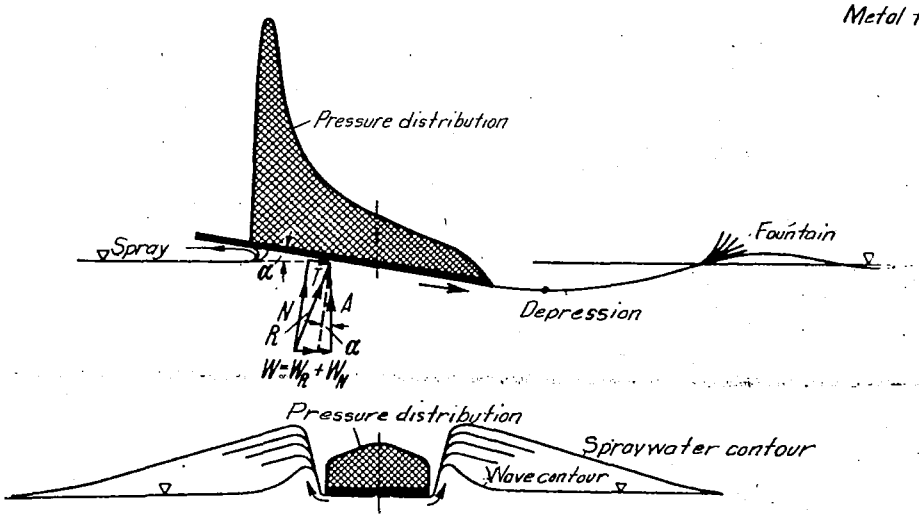

Figure 3.- Planing surface during planing process.

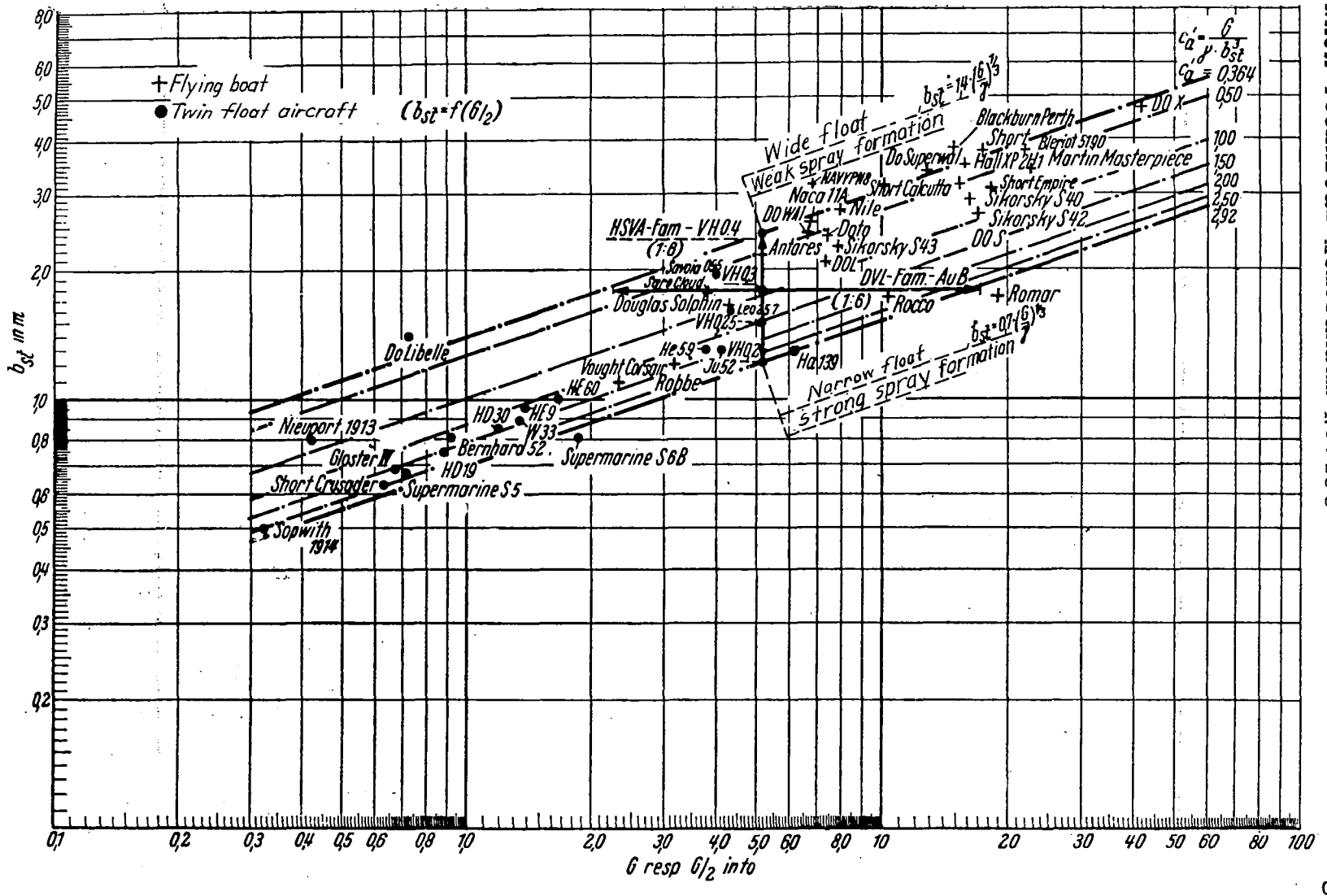

Figure 4.- Beam at step of aircraft as function of weight in flight.

Fig. 4

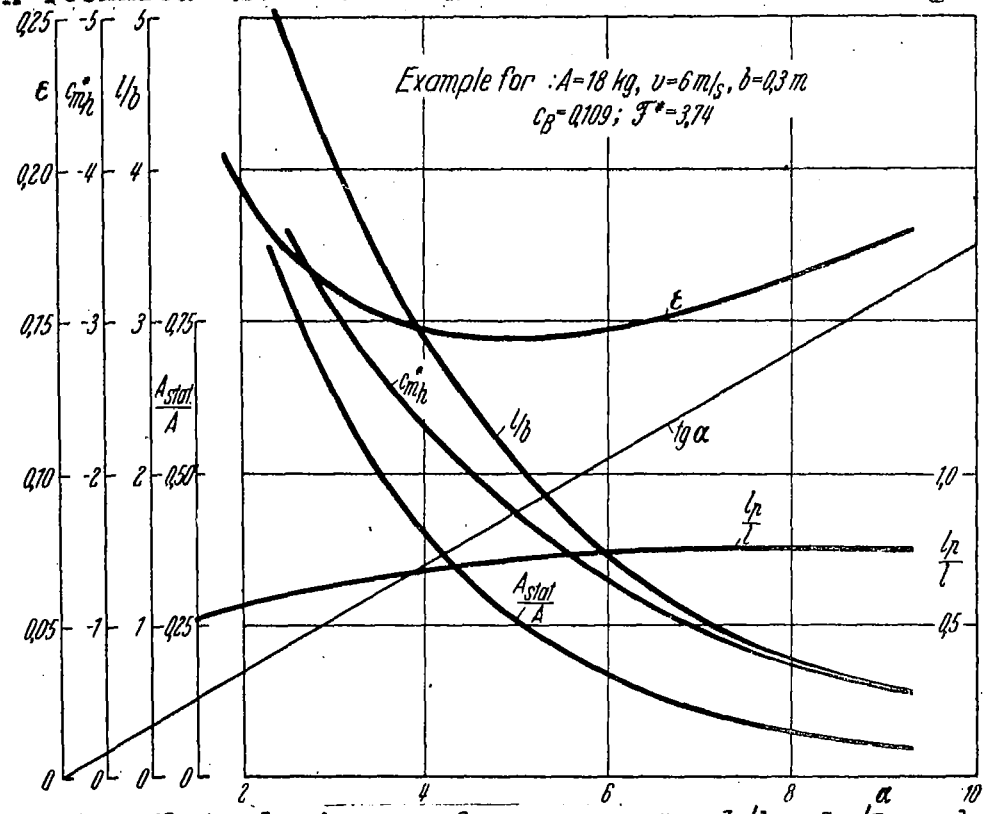

Figure 5.- Flat planing surface ε, c_{mh}^*, l/b, l_p/l and A_{stat}/A as functions of α.

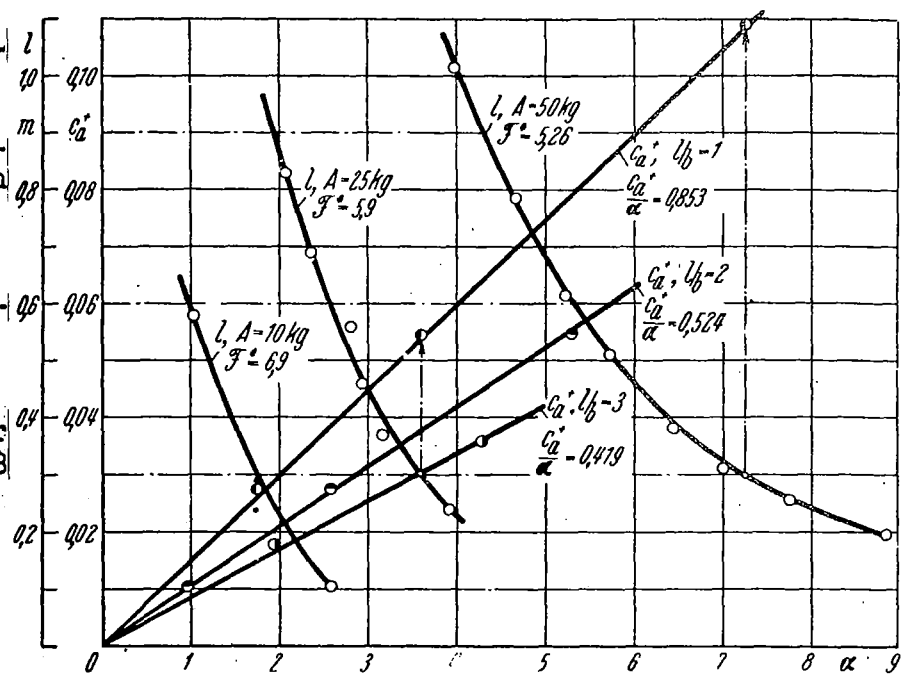

Figure 8.- Proof of relation $dc_a^*/d\alpha$ = const in region of high F^* numbers for flat rectangular planing surface. l as a function of α with A as parameter tests 16, 18 and 19; c_a^* as function of α with l/b = 1, 2, and 3 as parameter.

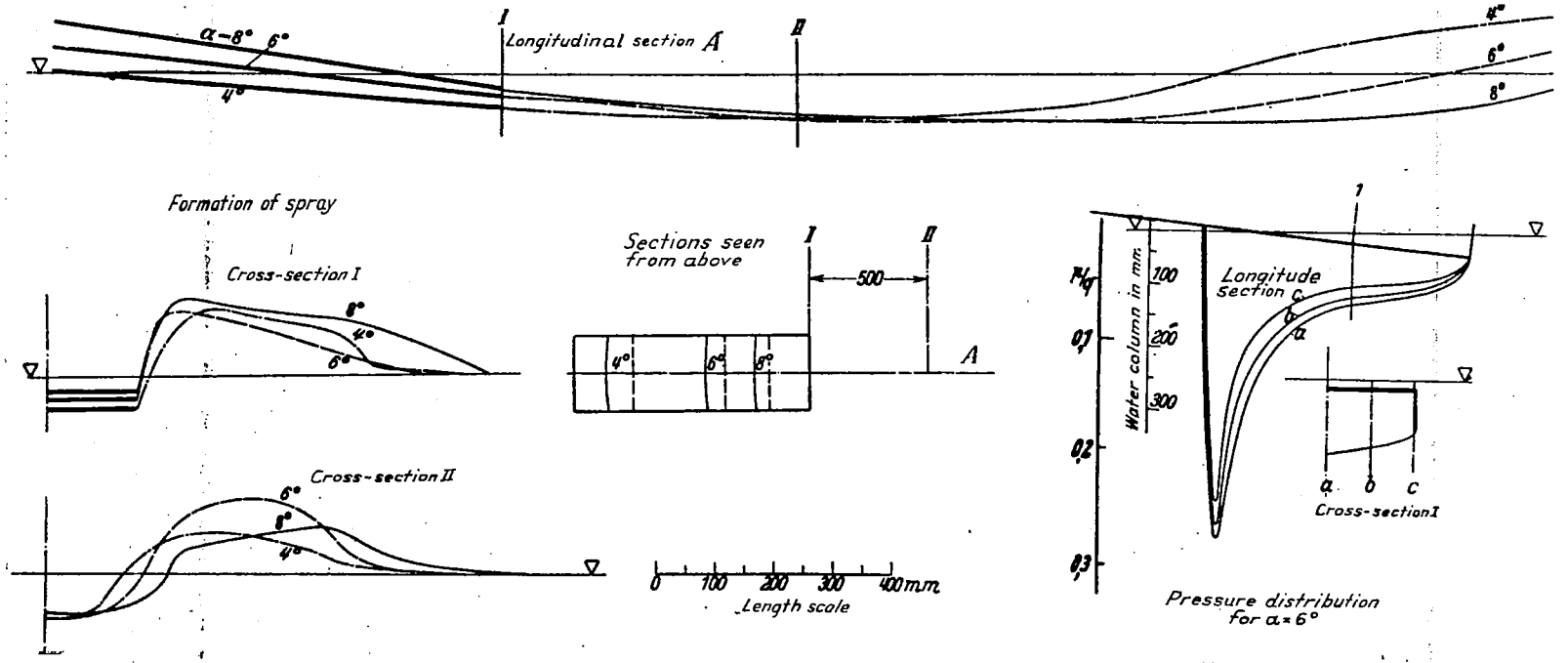

Figure 6.- Pressure distribution and flow picture of flat planing surface of 0.3 m width for A = 18 kg and v = 6 m/s.

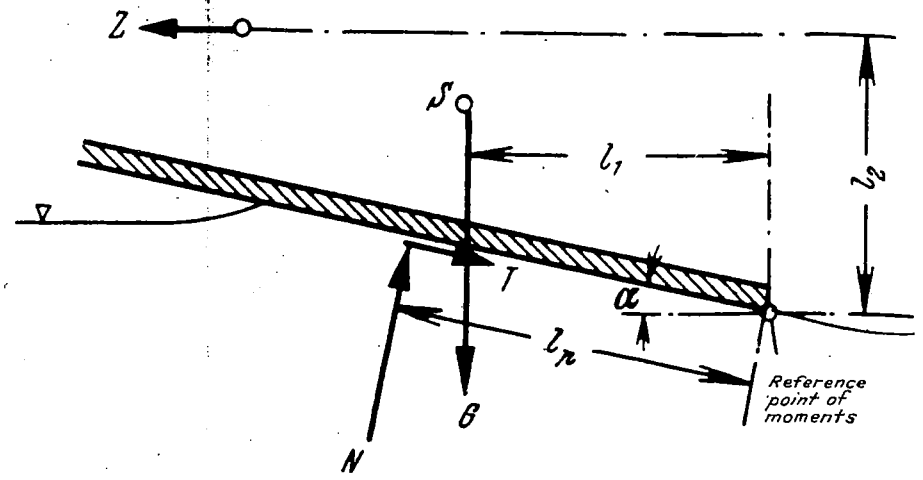

Figure 7.- Diagram for computing moment.

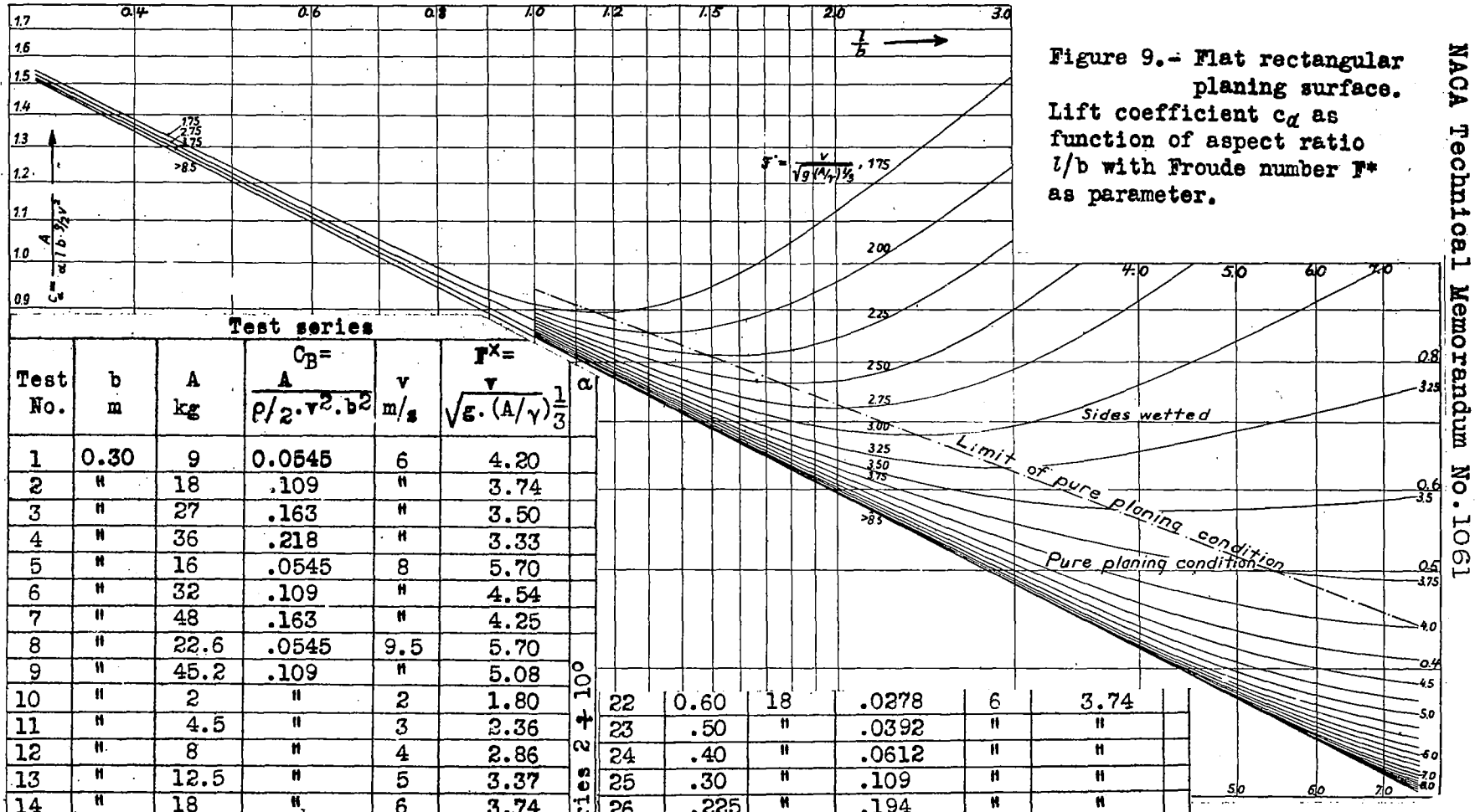

Figure 9.- Flat rectangular planing surface. Lift coefficient c_α as function of aspect ratio l/b with Froude number F^* as parameter.

Test series

Test No.	b m	A kg	$C_B = \frac{A}{\rho/2 \cdot v^2 \cdot b^2}$	v m/s	$F^x = \frac{v}{\sqrt{g \cdot (A/\gamma)^{\frac{1}{3}}}}$	α
1	0.30	9	0.0545	6	4.20	Varies 2 to 10°
2	"	18	.109	"	3.74	
3	"	27	.163	"	3.50	
4	"	36	.218	"	3.33	
5	"	16	.0545	8	5.70	
6	"	32	.109	"	4.54	
7	"	48	.163	"	4.25	
8	"	22.6	.0545	9.5	5.70	
9	"	45.2	.109	"	5.08	
10	"	2	"	2	1.80	
11	"	4.5	"	3	2.36	
12	"	8	"	4	2.86	
13	"	12.5	"	5	3.37	
14	"	18	"	6	3.74	
15	"	32	"	8	4.55	
16	"	50	"	10	5.25	
17	"	72	"	12	5.94	
18	"	10	0.0278	10	6.90	
19	"	25	.0545	"	5.90	
20	"	100	.278	"	4.70	
21	"	150	.327		4.38	
22	0.60	18	.0278	6	3.74	
23	.50	"	.0392	"	"	
24	.40	"	.0612	"	"	
25	.30	"	.109	"	"	
26	.225	"	.194	"	"	
27	.15	"	.435	"	"	
28	.60	144	.109	848	"	
29	.30	18	"	6	"	
30	.225	7.6	"	5.2	"	
31	.15	2.25	"	4.24	"	
32	.10	0.66	"	3.46	"	
33	.075	0.28	"	3	"	

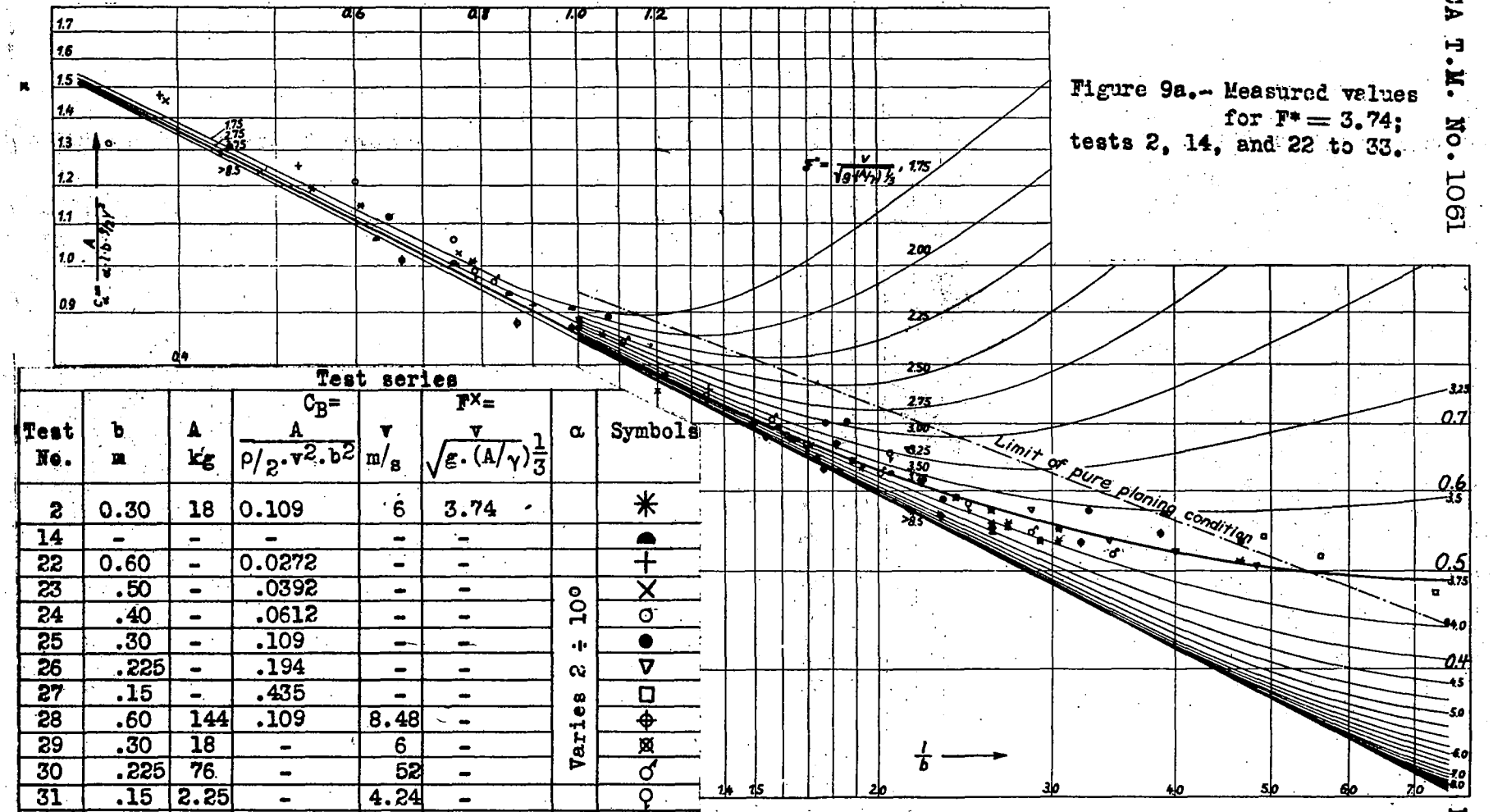

Figure 9a.- Measured values for $F^* = 3.74$; tests 2, 14, and 22 to 33.

Fig. 9a

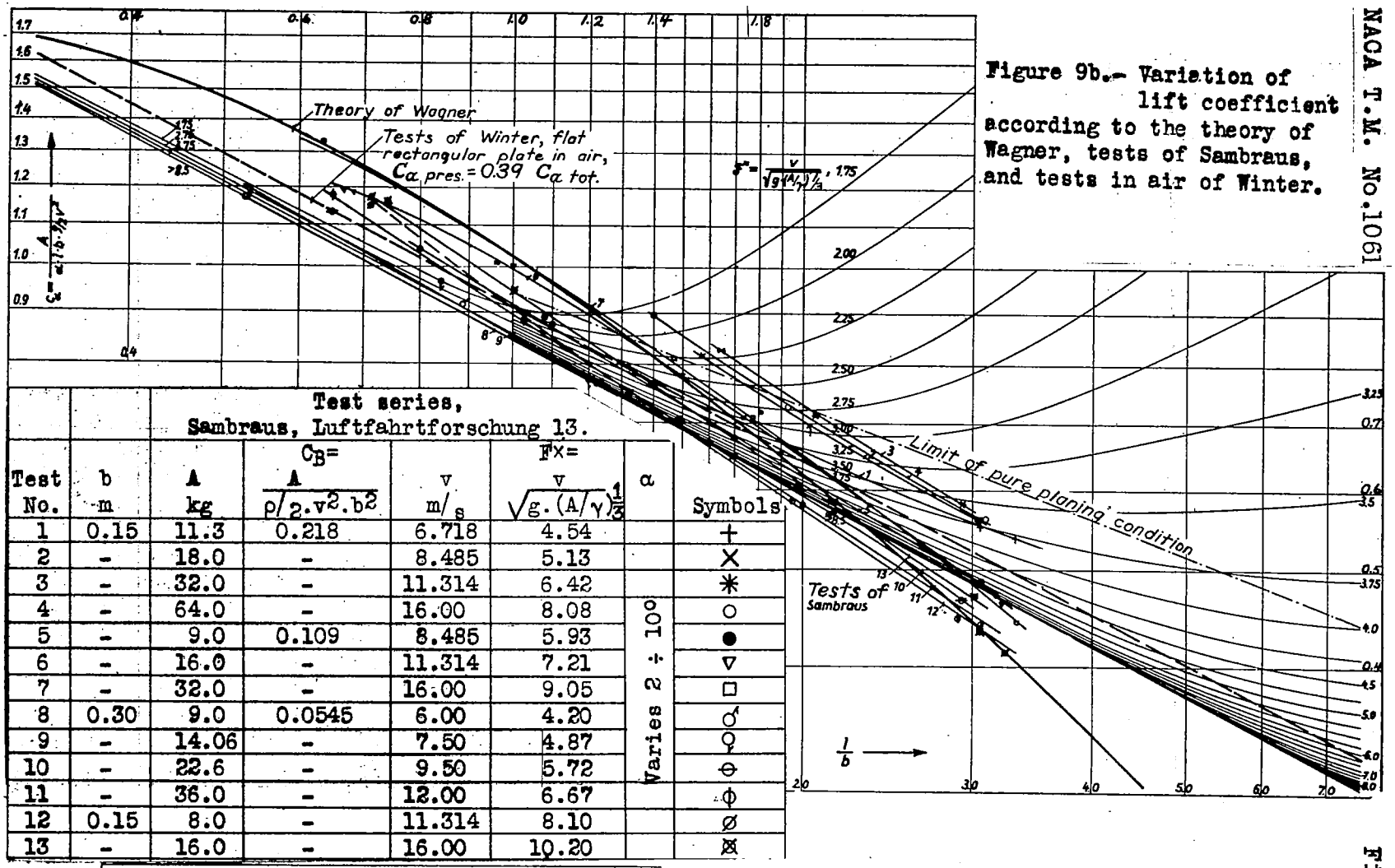

Figure 9b.- Variation of lift coefficient according to the theory of Wagner, tests of Sambraus, and tests in air of Winter.

Test No.	b m	A kg	$C_B = \frac{A}{\rho/2 \cdot v^2 \cdot b^2}$	v m/s	$F = \frac{v}{\sqrt{g \cdot (A/\gamma)^{1/3}}}$	α	Symbols
Test series, Sambraus, Luftfahrtforschung 13.							
1	0.15	11.3	0.218	6.718	4.54		+
2	-	18.0	-	8.485	5.13		×
3	-	32.0	-	11.314	6.42		✳
4	-	64.0	-	16.00	8.08		○
5	-	9.0	0.109	8.485	5.93		●
6	-	16.0	-	11.314	7.21		▽
7	-	32.0	-	16.00	9.05		□
8	0.30	9.0	0.0545	6.00	4.20		♂
9	-	14.06	-	7.50	4.87		♀
10	-	22.6	-	9.50	5.72		⊕
11	-	36.0	-	12.00	6.67	Varies 2 ÷ 10°	⊕
12	0.15	8.0	-	11.314	8.10		⌀
13	-	16.0	-	16.00	10.20		⊠

Tests of Winter, flat rectangular plate, V.D.I. Forschung Nos. 1 and 2.

l/b	0.50	0.666	0.80	1.00	1.50	2.00	2.86	7.46
F = 0.500 m^2	v = 28 m/sec			α = 10°				

Fig. 9b

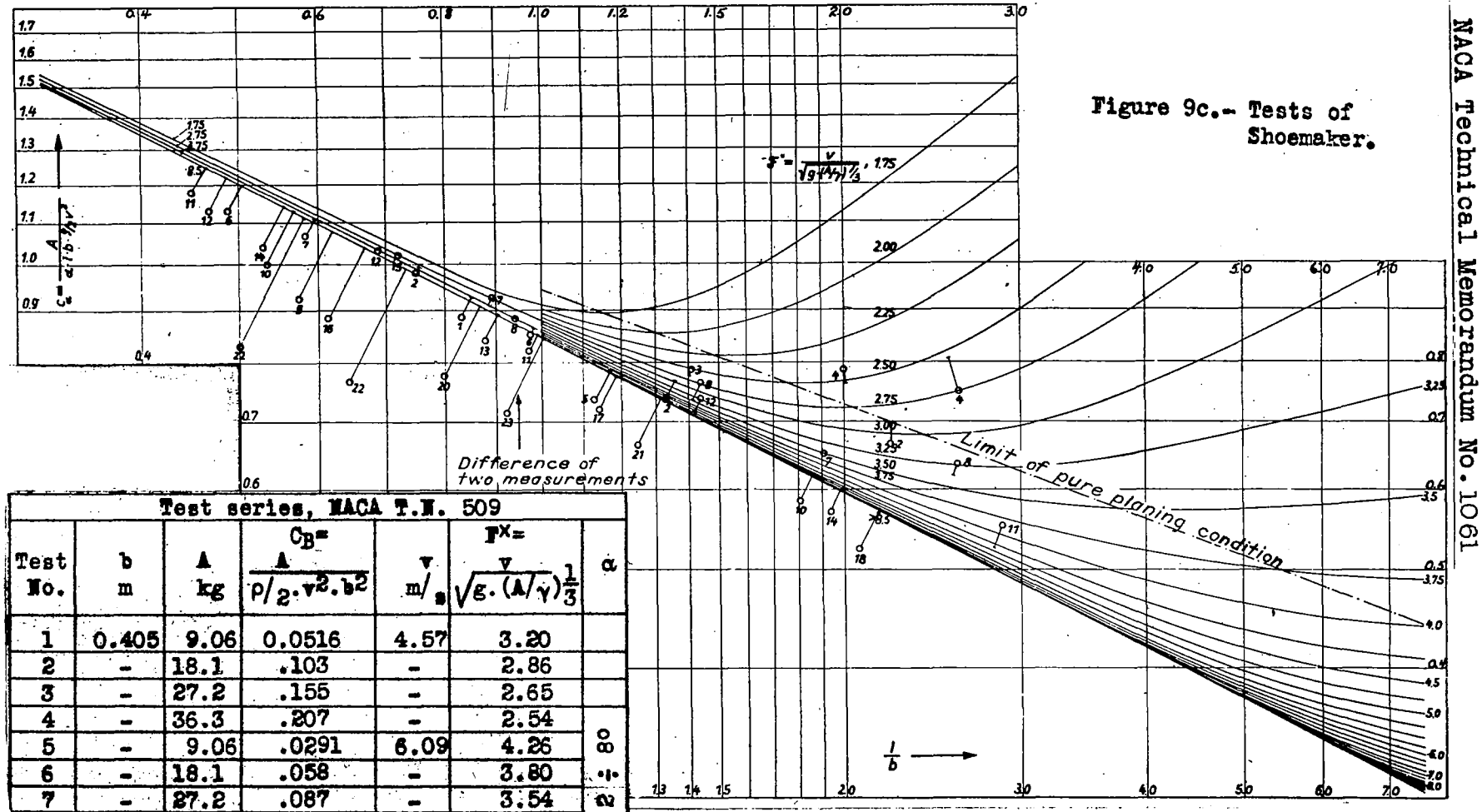

Figure 9c.- Tests of Shoemaker.

Test series, NACA T.N. 509						
Test No.	b m	A kg	$C_B = \frac{A}{\rho/2 \cdot v^2 \cdot b^2}$	v m/s	$F^x = \frac{v}{\sqrt{g \cdot (A/\gamma)^{1/3}}}$	α
1	0.405	9.06	0.0516	4.57	3.20	
2	-	18.1	.103	-	2.86	
3	-	27.2	.155	-	2.65	
4	-	36.3	.207	-	2.54	
5	-	9.06	.0291	6.09	4.26	Varies 2° to 8°
6	-	18.1	.058	-	3.80	
7	-	27.2	.087	-	3.54	
8	-	36.3	.116	-	3.38	
9	-	9.06	.0186	7.62	5.33	
10	-	18.1	.0372	-	4.76	
11	-	27.2	.0554	-	4.43	
12	-	36.3	.0746	-	4.31	
13	-	18.1	.0258	9.14	5.72	
14	-	27.2	.0388	-	5.31	
15	-	36.3	.0518	-	5.09	
16	0.405	18.1	.0189	10.67	6.66	
17	-	27.2	.0284	-	6.18	
18	-	36.3	.0379	-	5.92	
19	-	18.1	.0145	12.19	7.62	
20	-	27.2	.0218	-	7.08	
21	-	36.3	.0291	-	6.77	
22	-	27.2	.0172	13.72	7.96	
23	-	36.3	.0230	-	7.62	

Fig. 9c

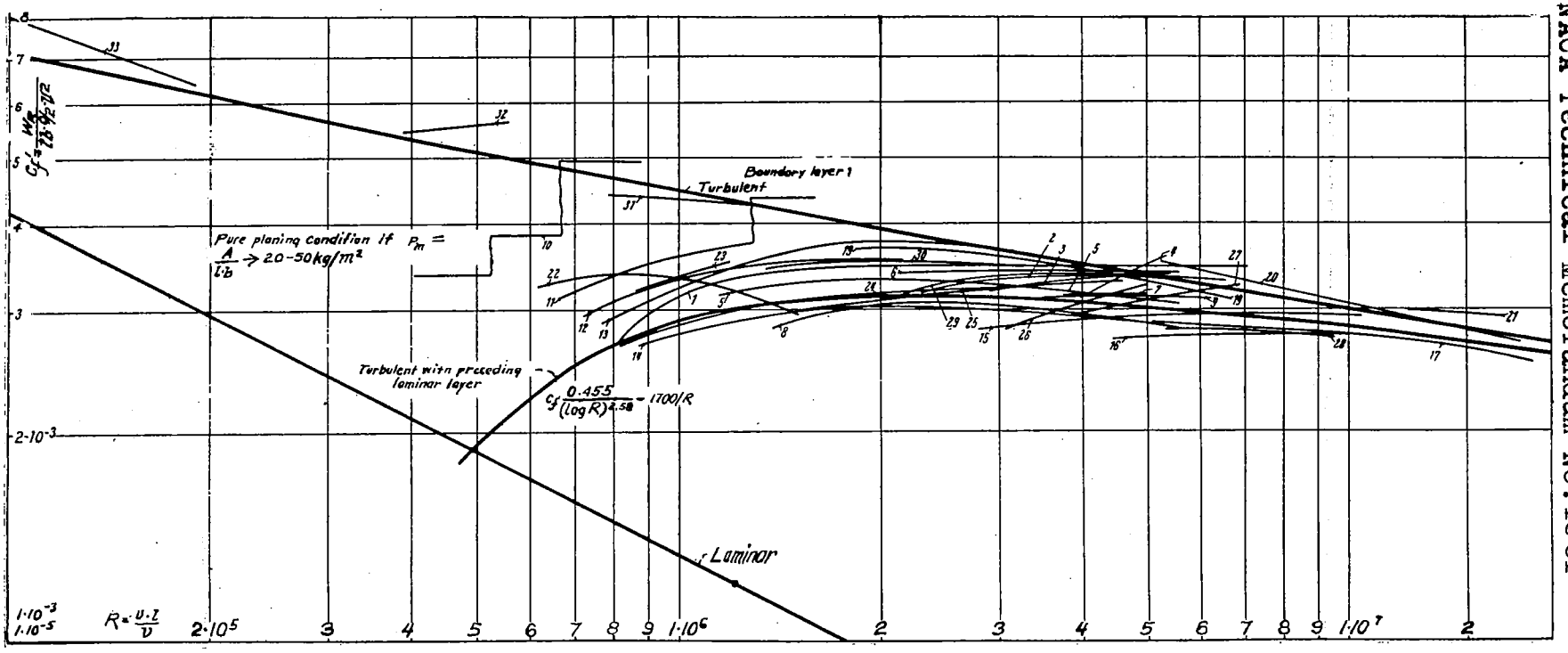

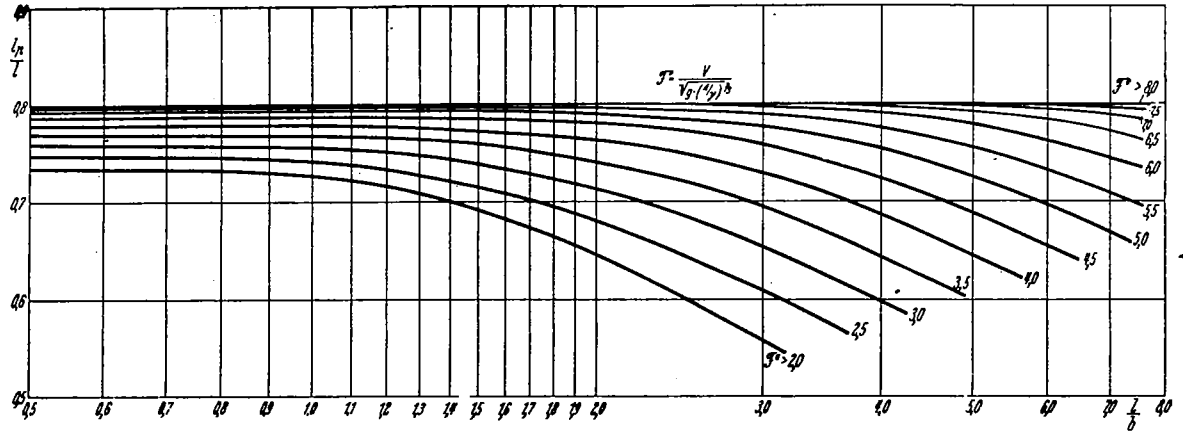

Figure 10.- Frictional coefficient c_f' as function of Reynolds number R. Mean values of test series 1 to 33. Flat rectangular planing surface.

Figure 11.- Center of pressure position l_p/l as function of aspect ratio l/b with Froude number F^* as parameter. Flat rectangular planing surface.

Figs. 10,11

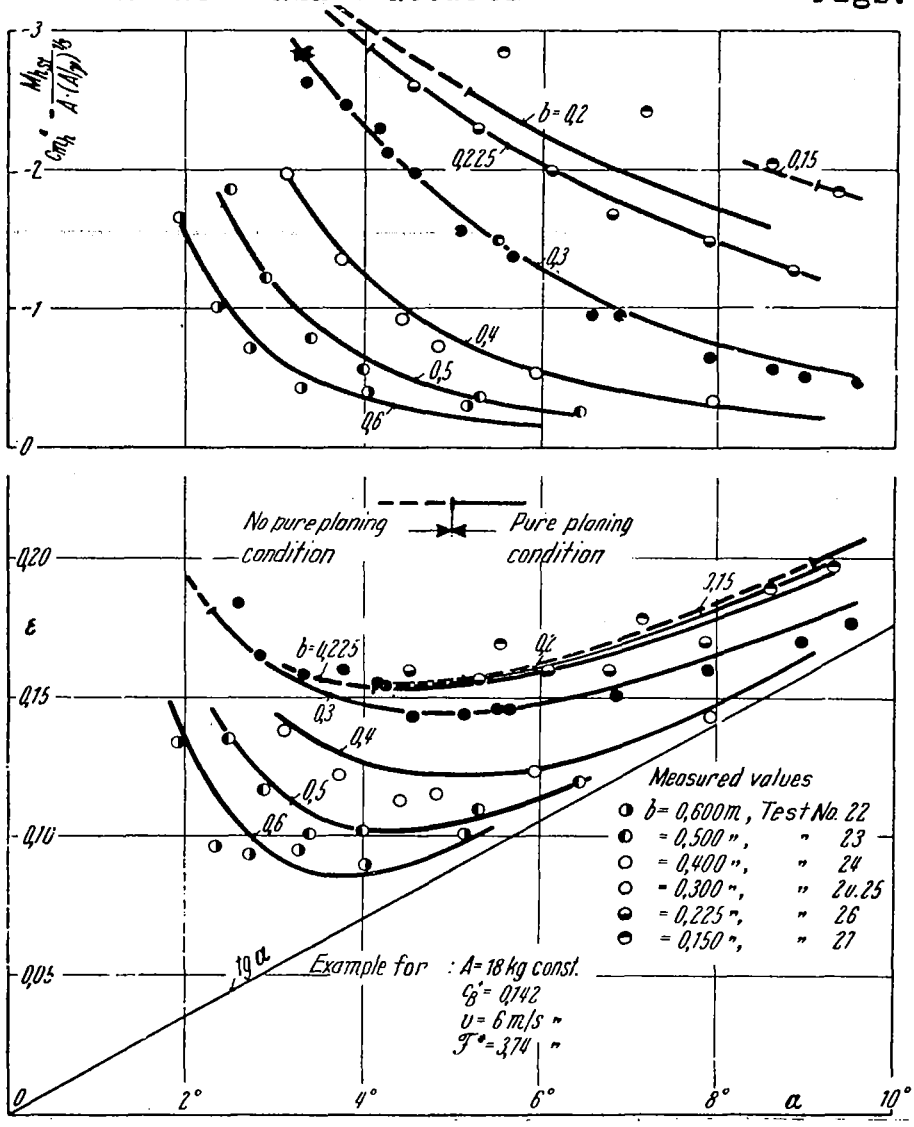

Figure 12.- Flat planing surface. Effect of beam ϵ and c_{mh}* as functions of α with b as parameter.

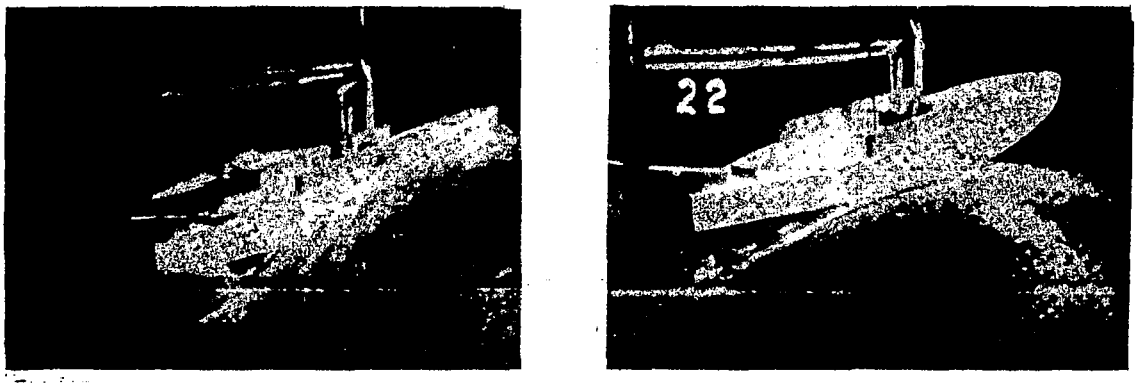

Figure 13.- Spray water comparison for model 0.2 percent (b_{st} = 0.2 m) and 0.4 percent (b_{st} = 0.4 m) for equal load A = 18 kg, speed v = 6 m/s and trim 6°.

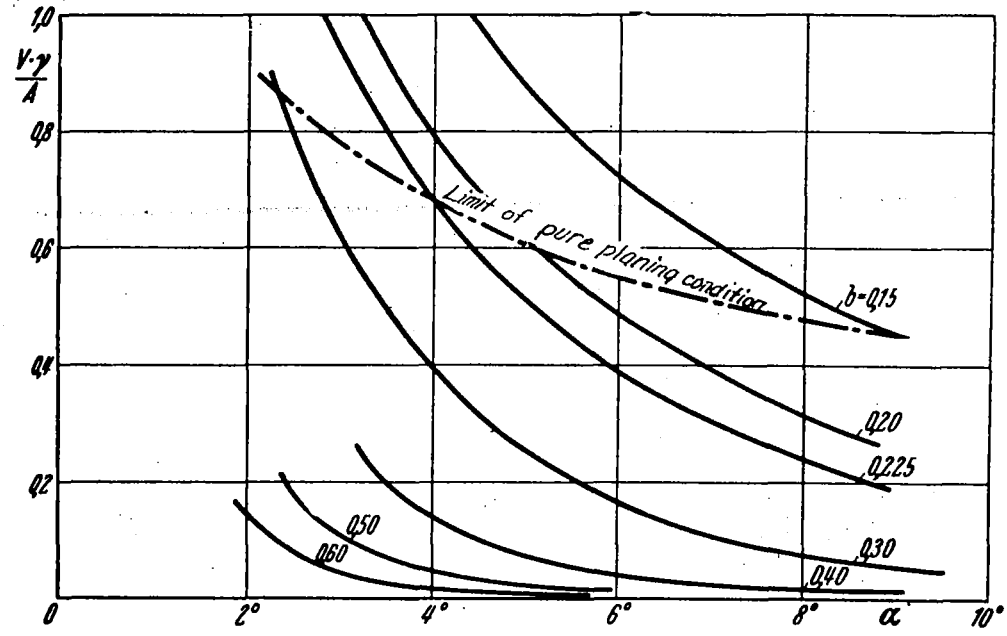

Figure 14.- Flat planing surface, effect of beam ratio of static displacement to total lift $V \cdot \gamma / A$ as function of trim angle α with b as parameter. $V = (\alpha \cdot l^2 \cdot b)/2$.

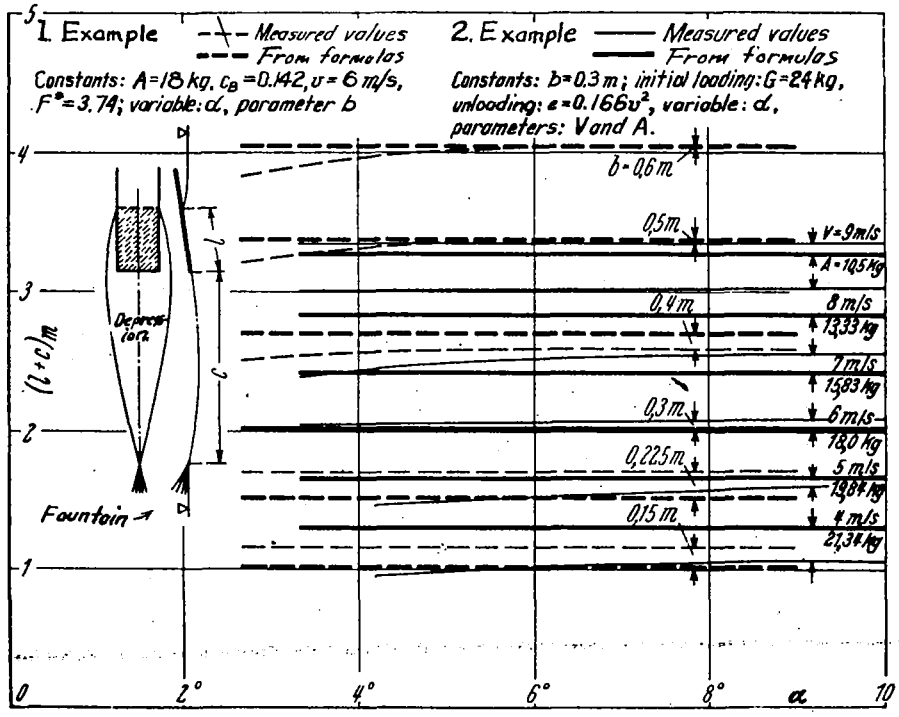

Figure 15.- Flat planing surface, position of fountain, $l + c = 1.8\ F^* b$.

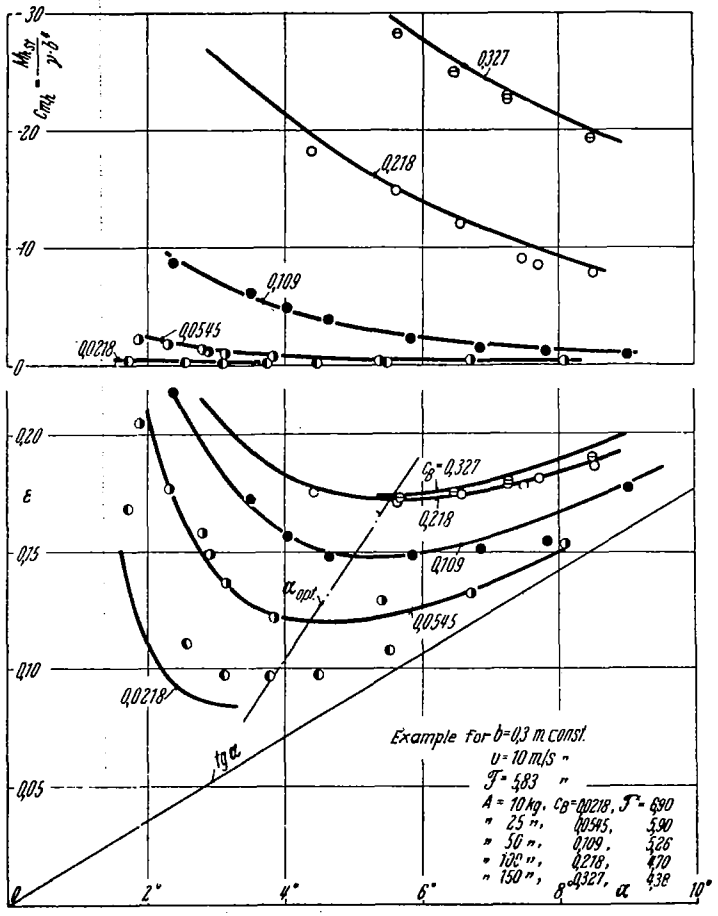

Figure 16.- Flat planing surface. Effect of load. ϵ and c_{mh} as functions of trim angle with c_B as parameter.

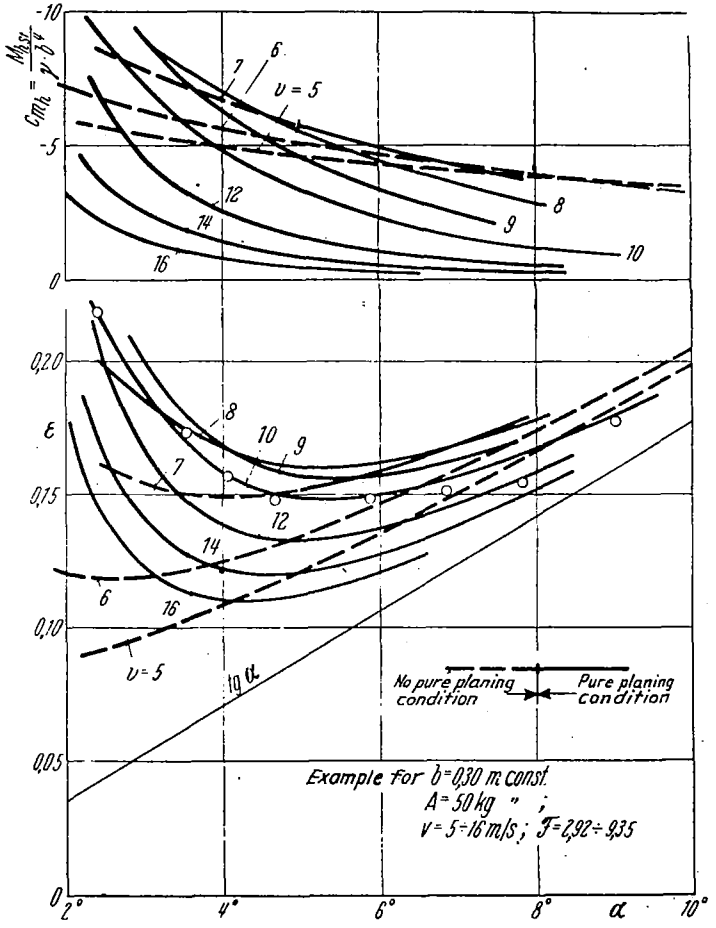

Figure 17.- Flat planing surface. Effect of speed. ϵ and c_{mh} as functions of α with v as parameter.

Figs. 16,17

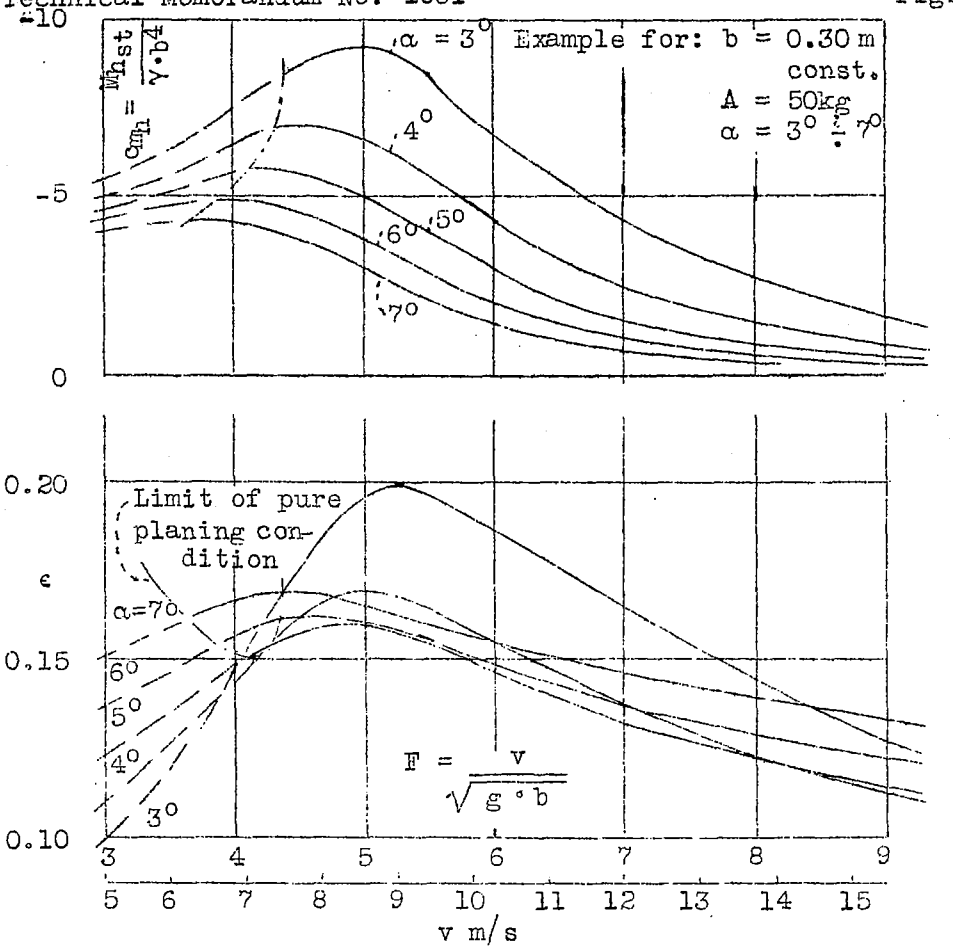

Figure 18.- Flat planing surface, effect of speed. ε and c_{mh} as functions of F with α as parameter.

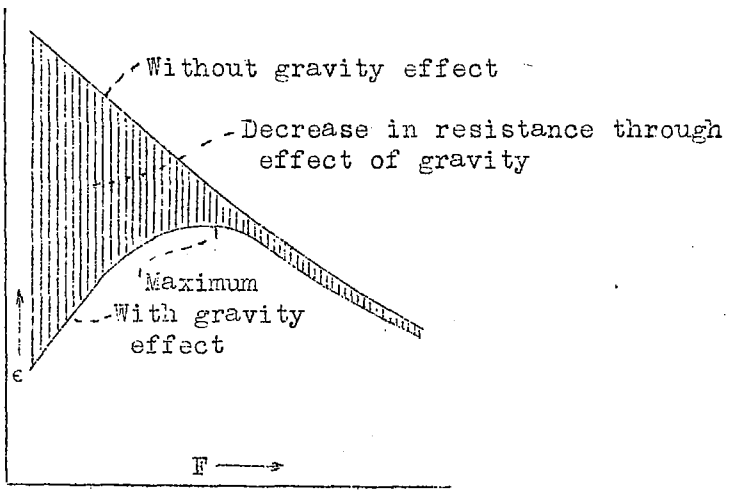

Figure 19.- Effect of gravity on the formation of the resistance maximum.

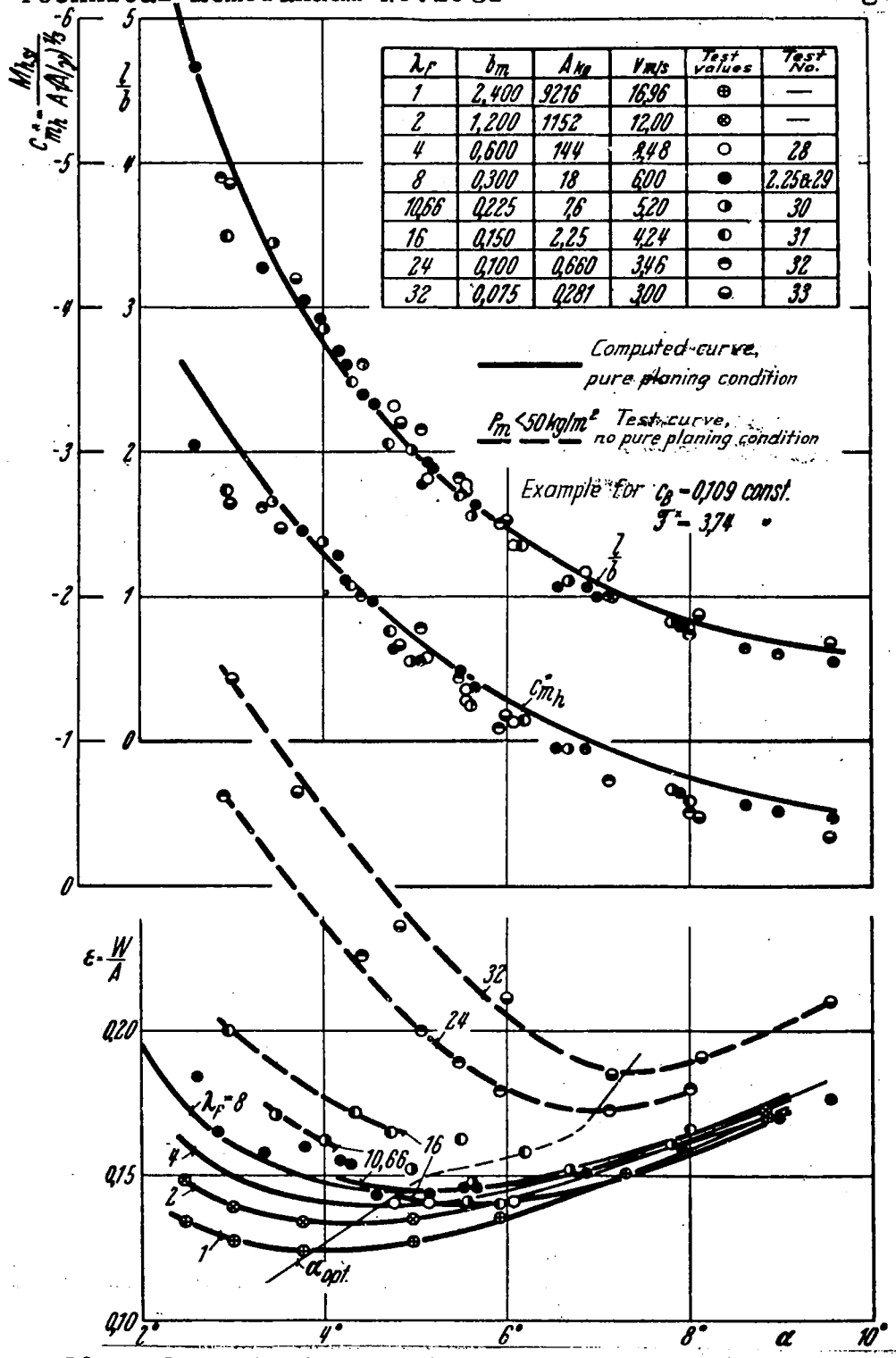

Figure 20.- Flat planing surface. Effect of scale. ϵ and c_{mh}* and l/b as functions of α with λ as parameter.

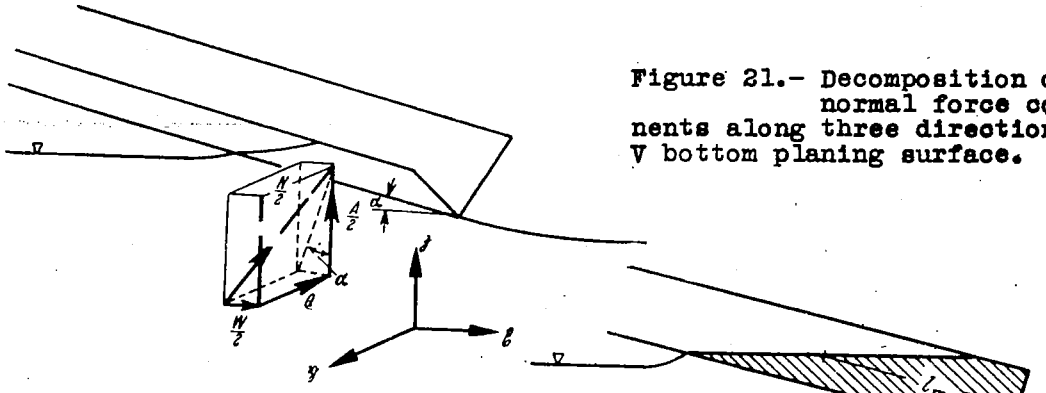

Figure 21.- Decomposition of normal force components along three directions for V bottom planing surface.

Figure 22.-"Pressure area" for V bottom planing surface.

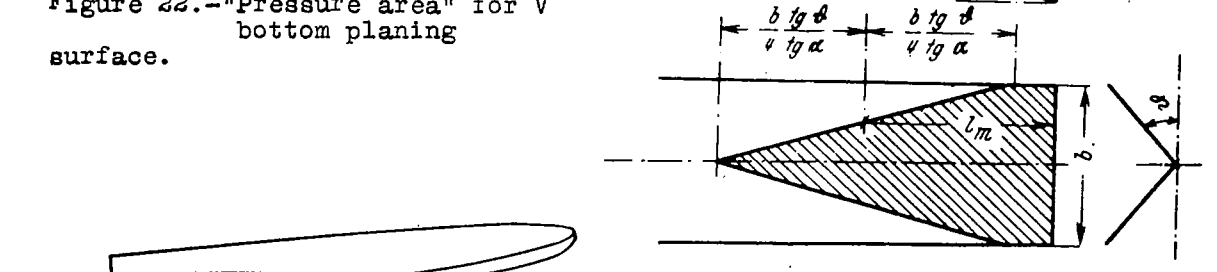

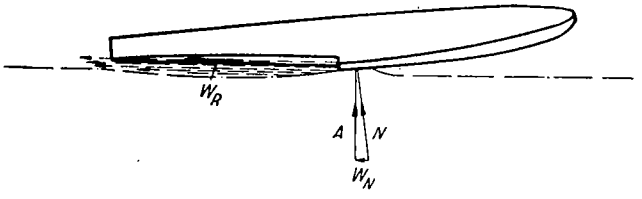

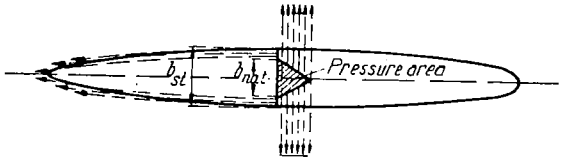

Figure 23.- Flow conditions before get-away.

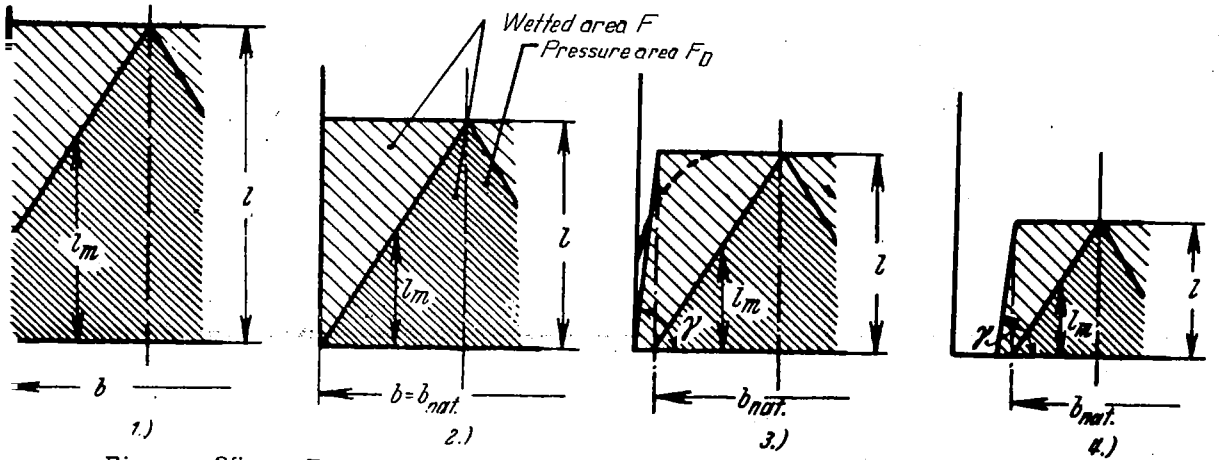

Figure 23a.- Pressure area and wetted area for V bottom surface.

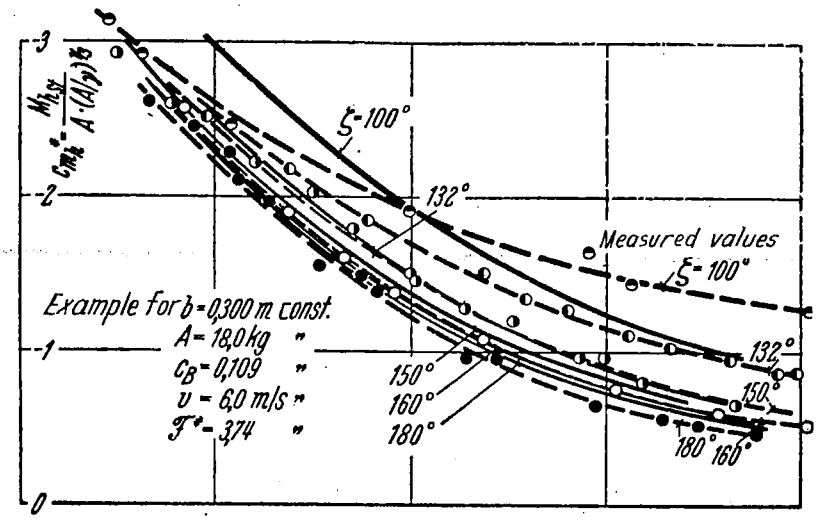

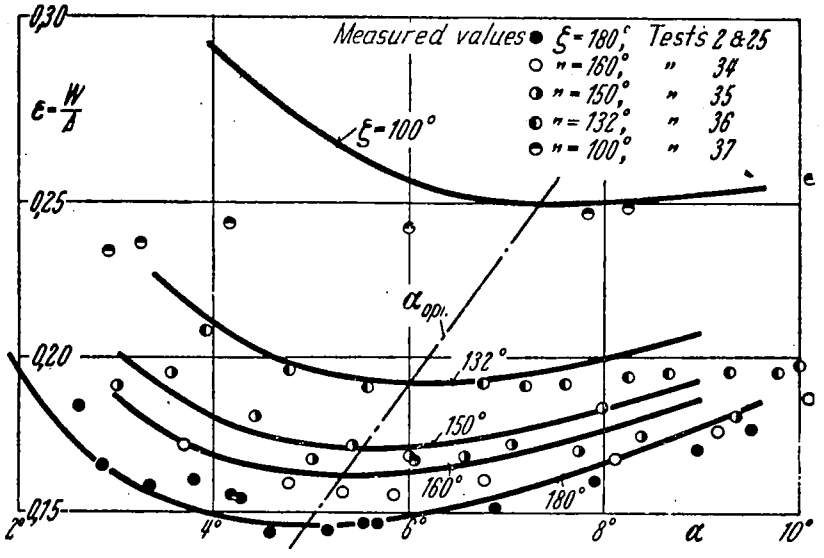

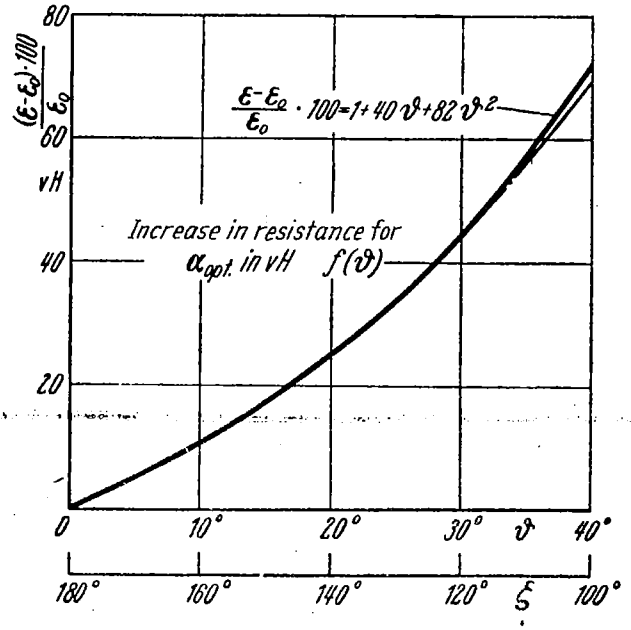

Figure 24.- V bottom planing surface. Effect of dead rise angle. ϵ and c_{mh}^* as functions of α with ζ as parameter.

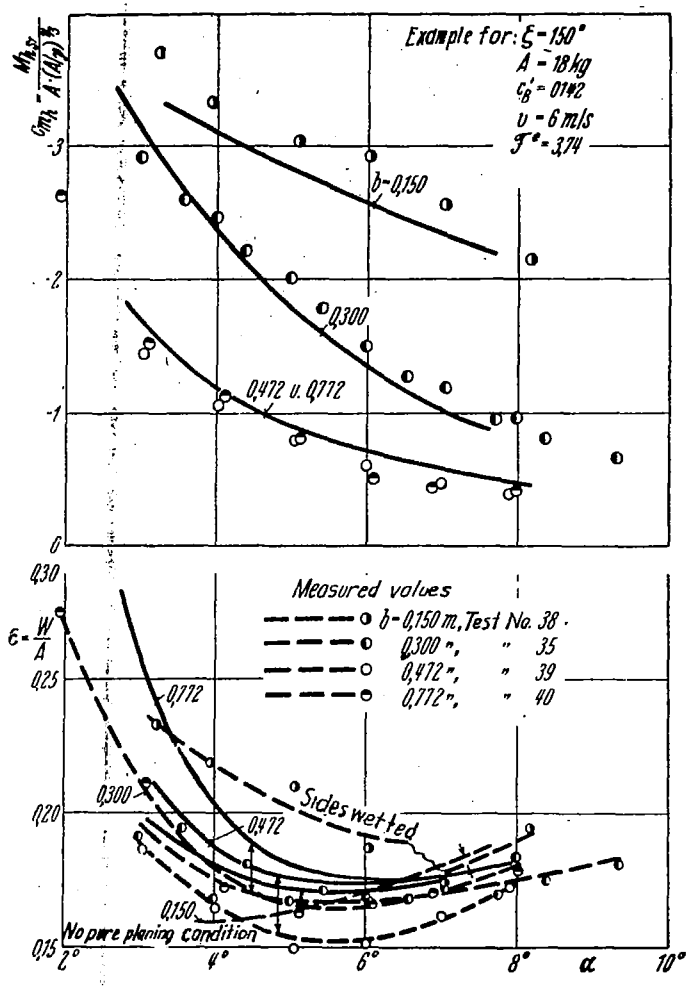

Figure 25.- V bottom planing surface. Effect of beam ϵ and c_{mh}* as functions of α with b as parameter.

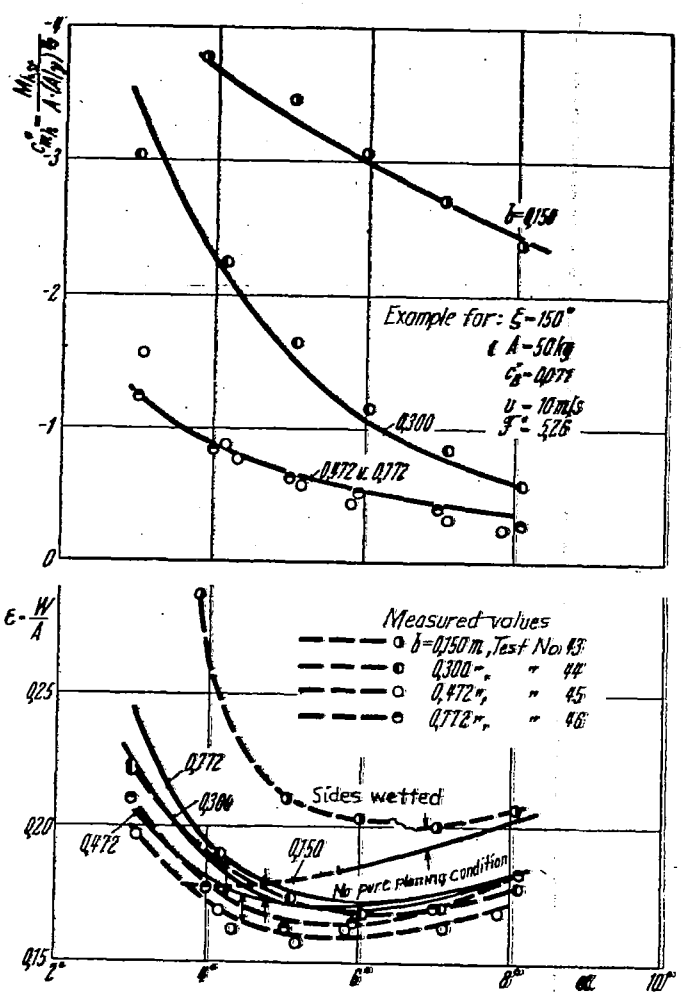

Figure 26.- V bottom planing surface. Effect of beam ϵ and c_{mh}* as functions of α with b as parameter.

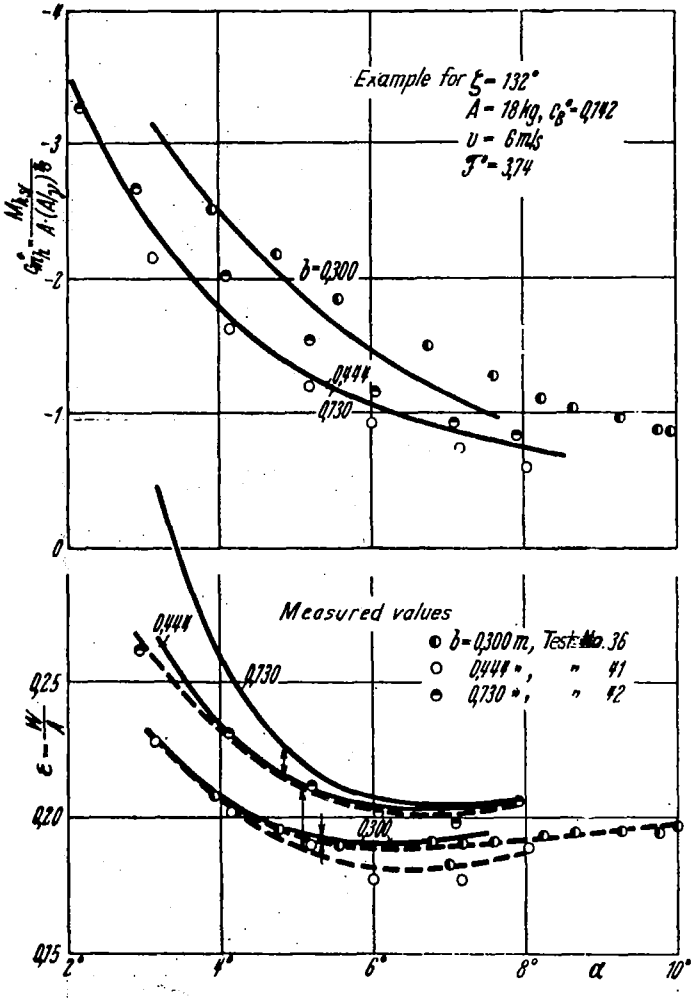

Figure 27.- V bottom planing surface. Effect of beam ε and c_{mh}* as functions of α with b as parameter.

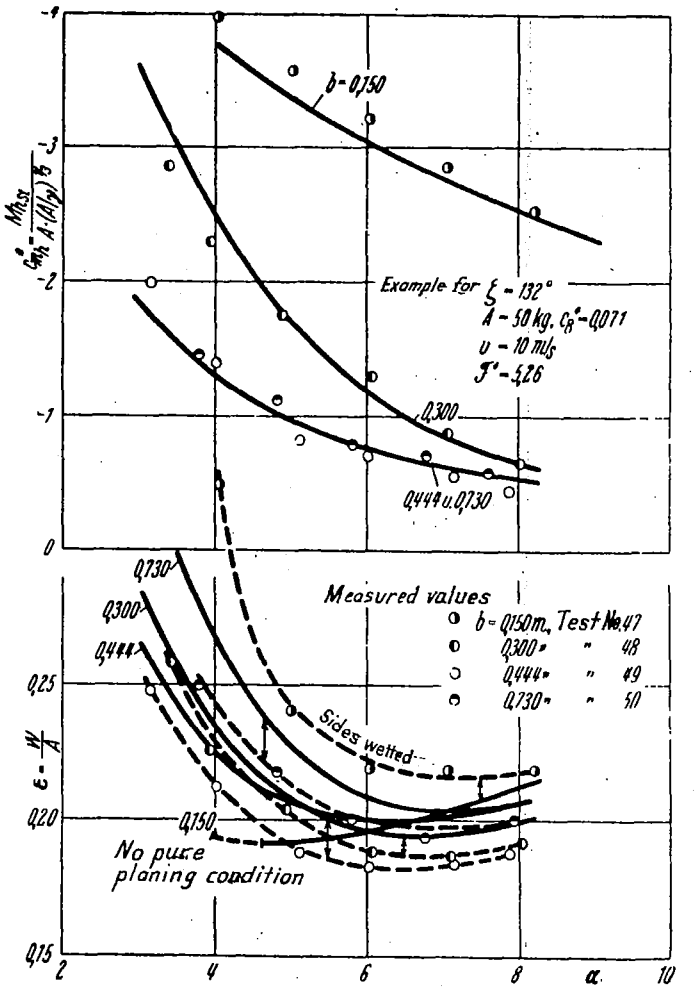

Figure 28.- V bottom planing surface. Effect of beam ε and c_{mh}* as functions of α with b as parameter.